An outer nuclear membrane protein promotes a polarized nuclear position and the future division plane during asymmetric cell division

M. Arif Ashraf[1], Le Liu[1,2], and Michelle R. Facette[1,*]
[1]Department of Biology, University of Massachusetts Amherst, Amherst, MA, USA
[2]Plant Biology Program, University of Massachusetts Amherst, Amherst, MA, USA

Orcid IDs:
MAA: orcid.org/0000-0002-0879-5835
LL: orcid.org/0000-0002-4262-5063
MRF: orcid.org/0000-0002-6214-9359

*Correspondence: mfacette@umass.edu

Author contributions: M.A.A. and M.R.F. conceived of the project and designed experiments. M.A.A. performed experiments and analyzed data, except stomatal conductance was performed by L.L.. M.A.A. and M.R.F. wrote the manuscript. M.R.F. supervised the project.

Abstract

Both plants and animals rely on asymmetric cell division to generate new cell types and is a core characteristic of multicellular organisms. Prior to asymmetric cell division, cell polarity is established. Cell polarity establishment and asymmetric cell division are universally important, although proteins important for polarity differ in plants and animals. *Zea mays* stomatal development serves as an excellent plant model system for asymmetric cell division, especially the asymmetric division of the subsidiary mother cell (SMC). In SMCs, the nucleus migrates to a polar location, after the accumulation of polarly localized proteins but before the appearance of the preprophase band. We examined a mutant of the outer nuclear membrane protein, which is part of the LINC (linker of nucleoskeleton and cytoskeleton) complex that localizes to the nuclear envelope in interphase cells. Previously, *mlks2* (*maize linc kash sine-like2*) were observed to have abnormal stomata. We confirmed these stomatal defects and used cell markers to pinpoint the precise defects that lead to abnormal asymmetric divisions. Proteins that are polarly localized in SMCs prior to division, including a polar accumulation of actin, polarize normally in *milks2* and remain polarized throughout and after division. However, polar localization of the nucleus is impaired, even in cells that have otherwise normal polarity. This leads to a misaligned preprophase band and atypical division planes Localization of MLKS2 revealed it is able to associate with mitotic structures, however the structure of the preprophase band, spindle and phragmoplast appeared normal in *mlks2.* Time-lapse imaging in *mlks2* revealed that the mutant had defects in pre-mitotic nuclear migration towards the polarized site, as well as an unstable position at the division site after formation of the preprophase band. Unpolarized nuclei lead to a misaligned preprophase band. Together, we show compelling genetic evidence that nuclear envelope proteins promote pre-mitotic nuclear migration and stable nuclear position, and that the position of the nucleus influences division plane establishment in asymmetrically dividing cells.

Keywords: Cell polarity, LINC complex, nuclear migration, asymmetric cell division, preprophase band, future division site determination

Introduction

The nucleus contains the genetic information inside the cell and it is separated from the cytoplasm through double lipid bilayer membranes. Proteins in the lipid bilayer membranes of nucleus are categorized as either outer nuclear membrane or inner nuclear membrane proteins based on their localizations. These nuclear membrane proteins help maintain the connection between nuclei and the rest of the cell. Because of the nature of this specific class of protein, they are known as LINC (Linker of nucleoskeleton and cytoskeleton) complexes. The LINC complex consists of KASH (Klarsicht, ANC-1, and SYNE homology) domain containing proteins in the outer membrane, and SUN (Sad-1/UNC-84) domain containing proteins in the inner membrane (Gumber, McKenna, Estrada, et al. 2019; Groves et al. 2020; Tapley and Starr 2013). KASH and SUN domains containing proteins interact with each other in the perinuclear space. Spatially, KASH domain containing proteins interact with cytoskeleton and SUN domain containing proteins are associated with nuclear lamins and chromatin (Supplemental Figure 1A). As a result, the LINC complexes relay signals and act as a vehicle for mechanosensing for the nucleus (Uzer, Rubin, and Rubin 2016; Fal et al. 2017). At the same time, the interaction of the cytoskeleton through the LINC complex facilitates nuclear movement. In plants, nuclear movement is an important during pollen and root hair growth, and during asymmetric cell divisions that occur during the formation of the zygote, lateral roots and stomata (Kawashima et al. 2014; Kimata et al. 2016; Barro et al. 2019; Muroyama, Gong, and Bergmann 2020; Gallagher and Smith 2000; Yi and Goshima 2020; Ashraf and Facette 2020; Brueggeman, Windham, and Nebenführ 2022). In the aforementioned cells, the nucleus takes on a polarized position, where its asymmetrical localization is a key part of the growth or division process.

During symmetric and asymmetric cell divisions, the cortical division zone, which later narrows to the cortical division site, is specified. The preprophase band (PPB) marks the cortical division zone at the G2/M transition, followed by other markers such as TRMs, TAN1, POKs, KCBP, RAN-GAP and MAP65-4 (Rasmussen and Bellinger 2018). Prior to the appearance of the PPB, the nucleus moves to the future division site. Symmetric divisions tend to follow geometrical rules, with the nucleus centered prior to division (Martinez et al. 2018; Moukhtar et al. 2019). Nuclear movement to the division site is especially apparent in asymmetric divisions. Nuclear movement prior to asymmetric cell division is stimulated by an intrinsic or extrinsic polarizing cue, and often results in the polarized accumulation of proteins or organelles (Li 2013). In some cases, asymmetrically dividing cells produce two volumetrically equal daughter cells and nuclear movement is not apparent (Facette, Rasmussen, and Van Norman 2019). In contrast, when an asymmetrically dividing cell yields two volumetrically distinct daughter

cells, nuclear movement is often visible prior to mitosis. Examples of volumetrically distinct plant cell divisions include the first asymmetric cell division of the zygote, protonemal branch formation, and stomatal divisions in grass and non-grass species (Kimata et al. 2016; Gallagher and Smith 2000; Ashraf and Facette 2020; Yi and Goshima 2020). Nuclear movement the polarized site can be actin or microtubule dependent (Ashraf and Facette 2020). Based on chemical approaches, it has been demonstrated that F-actin is crucial for the nuclear positioning during the first asymmetric division in zygote (Kimata et al. 2016). Both actin and microtubules are required for nuclear movement during asymmetric cell division in lateral root (Barro et al. 2019). Pre-mitotic nuclear migration is microtubule-dependent and post-mitotic nuclear movement is actin-dependent during Arabidopsis stomatal development (Muroyama, Gong, and Bergmann 2020). During protonema cell formation in moss (which lack a PPB), nuclear migration to the future division site requires microtubules (Yi and Goshima 2020). In stomatal subsidiary mother cells (SMCs), which are found in grasses such as maize and other monocots, chemical inhibitors have distinguished between the initial nuclear migration and maintenance of the nucleus at the future division site. Initial migration to the division site is actin-based and occurs in G1, while maintaining a polarized position requires microtubules (Panteris, Apostolakos, and Galatis 2006; Kennard and Cleary 1997). Together, these studies highlight that nuclear movements associated with asymmetric division are typical, yet are clearly controlled in different ways in different cell types. Moreover, movement of the nucleus happens prior to establishment of the cortical division site. This implies that nuclear position may feed into determining the future site of division. It has been shown that cells that lack a preprophase band (through genetic perturbation), can still correctly specify the cortical division zone, and while the newly formed cell wall may have a more variable angle, they are essentially correct (Schaefer et al., 2017). It has been suggested that the preprophase band may stabilize or reinforce the division site, rather than specify it (Livanos and Müller 2019). This implies that other cues feed into establishment of the cortical division site - but what are they? Nuclear positioning may be one of these cues. This is especially relevant in volumetrically distinct asymmetric divisions, where cues such as cell geometry may conflict with polarity cues.

Genetic perturbations that alter cellular polarity result in mislocalized nuclei, misaligned PPBs, and aberrant division planes during asymmetric divisions in several cell types (Gallagher and Smith 2000; Kimata et al. 2019). Physical displacement of the nucleus via centrifugal force can also result in misaligned PPBs (Murata and Wada 1991). These observations suggest that nuclear position can influence PPB placement. But, in these studies, cellular manipulation took place upstream (cell polarity establishment, organelle morphology, external cue) of the nuclear movement and PPB formation. For this reason, it is difficult to narrow down whether nuclear displacement

and PPB establishment are a consequence of cell polarity defect or alteration of organelle morphology or external physical cue? At this point, the role of nuclear position to influence the PPB placement is still a question to answer and it requires genetic and cell biology tools to manipulate the nuclear movement exclusively without hampering upstream cellular events.

To tackle this fundamental question, we have targeted LINC complex components from the outer nuclear membrane protein, known to interact with cytoskeleton, to eliminate the effect of upstream cellular events. In this study, we used a reverse genetics approach, where one of the outer nuclear membrane proteins and part of the LINC complex components, MLKS2 (Maize LINC KASH AtSINE-like), was examined during asymmetric cell division in maize stomatal development. Interestingly, single mutant of *mlks2*, *mlks2-1* and *mlks2-2,* has abnormal subsidiary cell, product of asymmetric cell division during stomatal development, phenotype and provided a great tool to dissect the role of outer nuclear membrane protein during asymmetric cell division. Our cell biology studies suggest that defects in nuclear polarization in *mlks2-1* mutant leads to the formation of misplaced PPB and subsequent mitotic apparatus (spindle, phragmoplast, and cytokinesis) follows the instruction of predetermined division plane information. Our work provides evidence that nuclear position promotes PPB placement and maintaining cortical division sites.

Results

MLKS2 is required for asymmetric cell division during stomatal development

Previously, it was shown that mutations in an outer nuclear membrane protein, MLKS2, causes defects during meiosis, pollen viability, nuclear shape, and stomatal development (Gumber, McKenna, Tolmie, et al. 2019). We reexamined two mu insertion lines, *mlks2-1* and *mlks2-2*, for stomatal phenotypes in expanded leaf 3 (Figure 1; Supplemental Figure S1). Consistent with previous results, both mutant alleles result in more aberrant subsidiary cells, extra interstomatal cells, and aborted guard mother cells in greenhouse-grown plants (Figures 1, B and C and Supplemental Figures S2, A-C). The number of aberrant cells varies depending on growth conditions and leaf number. Polarity mutants such as *pan1, pan2* and *brk1* have more abnormal stomatal cells in early-emerging leaves (unpublished data), while a previously characterized nuclear pore complex protein, *aladin1*, had more abnormal stomatal cells in late-emerging leaves (Best et al. 2021). To determine if *mlks2* mutants behave more similarly to polarity mutants vs *aladin1*, we analyzed stomatal cells in leaf 3, leaf 5, leaf 7 and leaf 10, where leaf 3 is the third leaf to emerge from the whorl (Supplemental Figure S3). There are more aberrant subsidiary cells in earlier-emerging leaves (leaf 3 and 5) than later

emerging leaves (leaf 7 and 10). Moreover, the frequency of aberrant subsidiary cells is higher in fast-growing summer field plants (12-22% in *mlks2-1* and 15-27% in *mlks2-2*) than slow-growing winter greenhouse grown plants (8-12% in *mlks2-1* and 9-16% in *mlks2-2*) (Figure 1;and Supplemental Figure S3). This indicates that faster growing plants in the summer field conditions have a higher frequency of aberrant subsidiary cells.

To further characterize the two alleles of *mlks2*, we created antibodies that target the N- (AA10-AA24) and C-terminal (AA454-AA474) region of MLKS2 (Supplemental Figure S1C). Both alleles have a Mu insertion in the exon 1, however *mlks2-2* is a stronger allele based on phenotypic data. It was previously shown that mRNA expression is reduced, not eliminated, in both alleles (Gumber, McKenna, Tolmie, et al. 2019). Western blot analysis suggests that both *mlks2-1* and *mlks2-2* alleles lack a 68kDa band corresponding to the predicted size of full length MLKS2 (Supplemental Figure S1D). Interestingly, the *mlks2-1* allele demonstrates an additional band of ~30kDa, which is missing in wild type and *mlks2-2* allele (Supplemental Figure S1D). A smaller protein of ~30kDa is consistent with the position of the transposon generating a truncated version of the protein containing amino acids 1-285.

In *A. thaliana*, the related protein, SINE2, is required for stomatal closure (Groves et al. 2020).To determine if MLKS2 is similarly required for stomatal closure, we used gas exchange to determine if *mlks2* plants were able to change stomatal conductance (i.e., close their stomata) in response to darkness using leaf 3 from greenhouse-grown plants. The mutant alleles responded similarly as wildtype (Supplemental Figure S4), suggesting that MLKS2 is not required for stomatal closure under our tested conditions.

MLKS2 localizes at the nuclear membrane and with the mitotic apparatus

Previously, it was shown that MLKS2 localizes to the plasma membrane, and this localization is dependent on the C-terminal transmembrane and KASH domains (Gumber, McKenna, Tolmie, et al. 2019). We repeated this expression analysis by transiently expressing MLKS2-mNeonGreen in tobacco pavement cells and also found a nuclear envelope localization (Figure 2A). Interestingly, previous studies demonstrated that ectopic expression of AtSUN1 (inner nuclear membrane protein and part of the LINC complex) not only localizes at the nuclear membrane, but also co-localizes with mitotic structures after nuclear envelope breakdown (Graumann and Evans 2011; Oda and Fukuda 2011). Since *mlks2* mutants have a defect in asymmetric cell division, we thought it was important to determine if MLKS2 can also localize to mitotic structures. We transiently expressed MLKS2 under a constitutive promoter in the tobacco leaf and observed nuclear membrane specific localization. To observe mitotic structures, we co-expressed pCaMV35S::AtCYCD3;1, which induces pavement cells to

undergo mitosis (Xu, Lee, and Liu 2020). Like SUN1, MLKS2 can also localize to the preprophase band, phragmoplast, and new cell plate (Figures 2, B-D, Supplemental Movie S1).

Polarized nuclear positioning, but not early polarity markers, are altered in *mlks2*

Proteins such as BRK1, PAN2 and PAN1 that are important for subsidiary cell polarization accumulate at the SMC-GMC interface, where the nucleus will eventually migrate (Figure 1A). Plants with mutations in genes encoding these proteins have defects in nuclear migration and polarized actin accumulation (Cartwright, Humphries, and Smith 2009; X. Zhang et al. 2012; Facette et al. 2015). Since nuclear migration occurs after polar accumulation of BRK1, PAN2 and PAN1, we predicted there would be no effect on their polarized localization. However, it is plausible that polarized nuclei may feedback to these polarity markers, and influence their localization. As predicted, all of these polarity markers are correctly localized in *mlks2.* Their polarized accumulation was maintained even after cell division in both wild type and *mlks2* (Supplemental Figure S5).

After the polarization of BRK1 and PAN proteins, the polarized accumulation of actin and nuclear migration to the future division site happen as concomitant steps (Facette et al. 2015). We predicted, based on the role of SUN-KASH proteins, that *mlks2* mutants likely have a role in nuclear migration to the future division site, prior to mitosis. To determine if nuclear position is altered in *mlks2* mutants, we used RanGAP-YFP, a nuclear envelope marker, to determine nuclear position in pre-mitotic SMCs. Nuclear polarization was categorized as: polarized (touching the cell wall, and centered relative to the GMC); offset (touching the cell wall, but not centered relative to the GMC); or unpolarized (not touching the cell wall) (Figure 3A). We observed a significantly higher number of offset and unpolarized nuclei in *mlks2-1* (Figures 3, B and C).

The role of the polarized actin patch is completely unknown. It might be tempting to speculate that the actin patch, which sometimes has actin cables radiating towards the nucleus, plays a role in nuclear polarization. However, several different experiments using cytological and/or inhibitor studies suggest this is unlikely (Apostolakos et al. 2018). Mutations in *brk1, pan2* or *pan1* each affect actin patch accumulation and nuclear migration. On a cell-by-cell basis, actin patch formation and nuclear polarization can be uncoupled, however to date no mutant has been shown to have an effect on only actin accumulation or nuclear polarization, or vice versa. The *mlks2* mutant provides a good genetic tool to untangle the relationship (or lack thereof) between actin accumulation and nuclear position. If nuclear polarization and polarized actin

accumulation are independent events, no effect on polarized actin accumulation is expected. However, if the nuclear position stimulates polarized actin accumulation, or the ARM domains of MLKS2 somehow stimulate actin patch formation independent of the nuclear position, actin accumulation at the polarized site might be abnormal. Using ABD2-YFP as a marker for actin, we quantified fluorescence intensity in *mlks2* mutants and wild type siblings at the polarized site and the adjacent cell wall in pre-mitotic SMCs, which is expressed as a ratio (Figure 5). SMCs were classified by their nuclear position. Similar to our analysis with RanGAP-YFP, *mlks2* mutants had more offset and unpolarized nuclei (Figure 5D). In both mutants and wild type SMCs, cells with polarized nuclei showed a higher fluorescence intensity (higher ratio) at the polarized site. However, no differences in the ratio of intensities were observed in *mlks2* mutants, relative to siblings, regardless of nuclear position. Importantly, we never observed a "delocalized" actin patch, which has been observed in *pan2* and *pan1* mutants (Cartwright et al., 2009; Zhang et al., 2012). In *pan* mutants, the actin patch will often spread to the adjacent cell walls. However, in *mlks2* mutants, even when the nuclei were unpolarized or offset, the actin patch was always enriched only at the GMC-SMC contact site (if present). Together, these data uncouple actin enrichment and nuclear positioning as independent events (Figure 4)

Preprophase bands are misaligned in *mlks2*

In *mlks2* mutants, BRK1, PAN2, and PAN1 are polarized throughout mitosis and after division. Therefore, despite a defect in nuclear polarization, the cell can still perceive and maintain polarity in *mlks2*. What leads to abnormal division planes in *mlks2?* Abnormal nuclear polarization in *mlks2* may lead to abnormal division planes, perhaps through the misplacement of mitotic structures. Alternatively, since MLKS2 can localize to mitotic structures after nuclear envelope breakdown, MLKS2 may have a direct role in the assembly or function of mitotic structures. We used CFP-TUB to examine mitotic structures in *mlks2* and wild type siblings (Figure 5; Supplemental Figure 6). No obvious structural deformation of the PPB (Figure 5A) or spindle (Supplemental Figure 6A) was observed in *mlks2-1*. But, we observed a number of transverse PPBs in *mlks2-1* (Figure 5A). Our quantification indicates that 8.5% (38/446 cells) of SMCs have a misoriented PPB in *mlks2*, while only 2.1% (7/338 cells) had a misoriented PPB in wild type siblings. Notably, the percentage of SMCs with a misoriented PPB correlates with the observed percentage of abnormal subsidiary cells (Figure 1). A similar correlation between the proportion of misaligned PPBs and aberrant subsidiary cells has been described in the polarity mutant *pan1* (Supplemental Figure 7) (Gallagher and Smith 2000). To determine if there was a relationship between PPB and nuclear position, we again classified nuclear position, but only in cells that had a PPB (Figure 5B). Notably, many cells with correctly aligned PPBs had offset nuclei, in

both wildtype (7% of SMCs) and *mlks2* (9%). However, in *mlks2* there were more plants with offset nuclei, and many of these cells also had a misaligned PPB - cells with both an offset nucleus and misaligned PPB occurred just 0.9% of the time in wild type, but 5.6% of the time in *mlks2.* We also observed more cells in *mlks2* that had an unpolarized nucleus and misaligned PPB (0.8% in wildtype, vs 2.0% in *mlks2).* Together, these data suggest that PPB alignment is abnormal in *mlks2*, and it closely correlates with nuclear position.

We also measured the mitotic spindle angle. Only spindles where one end was anchored at the GMC-SMC interface were measured. Although the mitotic spindle angle has a central tendency towards 90^0 in both wild type and *mlks2-1,* the mitotic spindle angle varies within a large range (30^0-170^0) in *mlks2-1,* which is statistically significant (Supplemental Figure 6B). This variation in angle could be caused by multiple mechanisms, which are not mutually exclusive. If the spindle orients perpendicularly to the axis of the PPB, as is typical in most divisions, the increased frequency of misaligned spindles would increase the observed range of angles. Alternatively, the spindle itself could be “wobbly”, and rotate during mitosis. Static images cannot resolve these possibilities. The final mitotic structure, the phragmoplast, also appeared misaligned in *mlks2* - however again, from static images it is impossible to resolve if the phragmoplast was misaligned relative to the PPB. Therefore we turned towards time-lapse imaging to clarify the effects of *mlks2* during mitosis.

Mitotic apparatus follows the initial division site marked by PPB

To determine the precise relationship between nuclear position, preprophase band placement, and final division plane we imaged SMCs undergoing mitosis. We had several important questions to address using our live imaging. Firstly, how is the position of the subsequent mitotic structures, the spindle and the phragmoplast, influenced by nuclear position and/or preprophase band in *mlks2*? Secondly, is the PPB position set with respect to the nuclear position? And once the PPB is formed, is the nuclear position stable? Can the PPB influence nuclear position? Thirdly, are offset and unpolarized nuclei mispositioned because their initial guidance towards the guard mother cell fails, or because their nuclear position at the division site is unstable? That is, how exactly does MLKS2 influence nuclear position?

We addressed these questions using both HIS-YFP and CFP-TUB markers in *mlks2-1* and wild type siblings. Histone helps to visualize the nuclear position and the transition through G1 to G2 phase while CFP-TUB facilitates the visualization of cell division events, such as PPB, mitotic spindle, phragmoplast, and cytokinesis. For this experiment, we used the meristematic region or leaf base of L4 and performed the time

lapse imaging in every 2 minutes interval (Figure 6A and Supplemental Movies S2 and S3). We observed the nuclear position and complete cell division (PPB to cytokinesis) from a total 62 cells (27 wild-type and 35 *mlks2-1* cells). In wild type cells, all of the PPBs were correctly aligned, and in 26/27 cells the nucleus was polarized when the PPB was present. Mid-plane views of mitosis and cytokinesis show that after PPB disassembly, the spindle forms perpendicular to the PPB, followed by the phragmoplast, which forms at the expected division site (Supplemental Movie 2). In one wild type cell, the nucleus was offset, however PPB, spindle and phragmoplast positioning was normal. In the *mlks2* mutant, 10/25 cells had a misaligned PPB, and in all 10 of these cells the nucleus was either offset (6 cells) or unpolarized (4 cells). In all cases, the spindle and phragmoplast orientation matched the orientation of the PPB, suggesting the defect is in PPB positioning. Supplemental Movie S3 shows a *mlks2* SMC where the nucleus is initially offset, and the PPB is transverse to the axis of the cell. The spindle shows an oblique angle, and is neither perpendicular to the GMC-SMC interphase, nor the PPB. The phragmoplast aligns with the former PPB position. We measured the total time for mitosis, and found that metaphase and anaphase timing are similar between perfectly oriented and misoriented cell division (Supplemental Figure 8A); but telophase and cytokinesis require longer time during misoriented cell division (Supplemental Figure 8B). The longer time requirement for misoriented mitosis during telophase and cytokinesis is due to the longer path covered by transversely formed phragmoplast (Supplemental Figures 8, C and D). Together, these data suggest that spindle and phragmoplast position are not directly affected, but rather their misalignment is a result of aberrant PPB positioning.

What is the relationship between PPB position and nuclear position? As suggested by our static image data and Supplemental Movie S3, nuclear position influences PPB position. But, can the PPB influence nuclear position, and how stable is nuclear position after PPB formation? In wild type cells, the nucleus shows very little movement after PPB formation (Supplemental Movie S4). Supplemental Movie S5 shows a *mlks2* SMC where the nucleus is unpolarized, although biased towards the GMC. The PPB shows a transverse localization. The nucleus centers itself within the PPB, prior to nuclear envelope breakdown. However, we also saw examples where the nuclear position was unstable in mutant cells after the PPB was formed. Supplemental Movie S6 shows a *mlks2* SMC with a normally oriented PPB, however the nucleus moves away from its polarized position. We never observed this phenomenon in wild type cells. These data suggest that PPB can influence nuclear position, however in *mlks2* mutants nuclear position is not stable.

This partially answers our third question - what causes the underlying nuclear position? Nuclear migration to the future division site in SMCs happens in G1, well

before division (Kennard and Cleary 1997), and takes many hours. Our imaging requires dissection of the undeveloped maize leaves from the plants, thus imaging from migration to mitosis is not feasible. None-the-less, we were able to record pre-mitotic nuclear movements. In wild type, movement of the nucleus occurs steadily towards the polarized site, and once it moves towards the site does not move away (Supplemental Movie S7). In the mutant, we often observed “kiss-and-run” behavior, where the nucleus moves towards the GMC, and then away again (Supplemental Movie S8). Together, these data suggest that *mlks2* mutants have defects in both moving towards the division site, and maintaining the position, prior to and after PPB formation.

Discussion

Together, our data indicate that the nuclear position during volumetrically asymmetric divisions is important for establishment of the cortical division site (Figure 7). Positional cues from the nucleus feed into the orientation of the PPB, which then guides the orientation of the subsequent mitotic structures. Aberrant nuclear positioning results in misaligned PPBs and misaligned division planes (Figure 7).

Our data illustrate several key findings. Firstly, the nuclear envelope protein MLKS2 is important for nuclear movement to the future division site, and also for maintenance of the position at the division site. In a subset of cells, the nucleus was displaced at the onset of mitosis, even in otherwise polarized cells, which results in an abnormal specification of the division site and subsequent division. Notably, many cells still had correctly polarized nuclei. This could be for several reasons. MLKS2 has an orthologue, MLKS1 (Gumber, McKenna, Tolmie, et al. 2019). Double mutants may produce a more dramatic phenotype. Other nuclear envelope complexes, such as the nuclear pore, may also contribute to cytoskeletal interactions and nuclear positioning (Best et al. 2021). Previous inhibitor studies in maize indicate that pre-mitotic nuclear migration is driven by actin networks, while maintenance of a polarized position is driven by microtubule networks (Panteris, Apostolakos, and Galatis 2006). Notably, MLKS2 is involved in both migration and position maintenance.

A second key finding is that perturbation of nuclear position results in a misaligned PPB and subsequent asymmetric divisions, even in the presence of polarization cues. The misaligned PPBs typically took on a consistent, transverse orientation, suggesting that other cellular or extrinsic cues contribute to determining the PPB position in SMCs. Interestingly, many of the aberrant divisions took place in mutant cells where the nucleus was only slightly offset from the polarized position. In both wild type and mutant cells, offset nuclei occur 7-9% of the time, with completely normal PPB positioning. Why, in the mutant, do offset cells sometimes result in aberrant division site

specification, while in other cases it is normal? High resolution imaging of the nuclear envelope and cytoskeleton at the time of preprophase band establishment may help resolve this question. Indeed, understanding the events at the nuclear interface in general, may help resolve how exactly the nucleus, perhaps through nucleating events, promotes PPB positioning.

Notably, in Arabidopsis roots that lack a PPB through genetic manipulation, division planes are relatively normal (POK1 localization), as is overall tissue patterning (Schaefer et al. 2017). Specification of different cell layers in the Arabidopsis root occur via asymmetric division, however these asymmetric divisions tend to create volumetrically similarly sized cells. In Arabidopsis root asymmetric divisions, the nucleus fills much of the cell, and nuclear migration is not a prominent feature. Therefore, the cues independent of the nucleus and the PPB, including polarity and mechanical cues, may be at play to ensure correct asymmetric divisions. In non-PPB forming cells, such as caulonema tip cells of *Physcomitrella patens*, cortical division site marker PpKin12-Is, (homologs of AtPOKs), localize at the cortical division zone (Yi and Goshima 2020; Miki et al. 2014). Hence, PPB-devoid cells can perfectly maintain the future division site through localizing cortical division zone specific proteins. Division plane establishment is an essential and complex feature that likely has many combinatorial factors, therefore the context of cell division must always be considered. In volumetrically asymmetric divisions, such as in the SMC, nuclear position and PPB establishment appear to be especially important.

Materials and Methods

Plant materials

Stably expressed fluorescent marker lines: BRICK1-CFP (Facette et al. 2015), PAN2-YFP (X. Zhang et al. 2012), PAN1-YFP (Humphries et al. 2011), FIMBRIN (ABD2-2xYFP), CFP-TUBULIN-BETA (Mohanty et al. 2009), TUBULIN-YFP (Mohanty et al. 2009), HISTONE H1B-YFP (Mohanty et al. 2009), TANGLED1-YFP (Martinez et al. 2017), RanGAP-YFP (obtained from MaizeGDB stock center; UWYO-FP032) were described previously (Krishnakumar et al. 2015). *mlks2-1* (mu1038603/UF-Mu04133) and *mlks2-2* (mu1058535/UF-Mu07312) mutant seeds were a gift from Hank Bass (Florida State University). *pan1-ems* was provided by Laurie Smith (University of California San Diego) and was described previously (Gallagher and Smith 2000). p35S::AtCYCD3;1 plasmid was generously shared by Bo Liu (University of California Davis) (Xu, Lee, and Liu 2020). Single and double fluorescent protein marker lines with *mlks2-1* and *mlks2-2* were generated through genetic crosses.

Plant growth condition

Plants used for experiments were grown for approximately 2 weeks in the greenhouse condition (temperature between 20°C to 29°C and 16h day length). For the field sample, plants were grown in the farm facility of the University of Massachusetts Amherst in the summer of 2021. For all experiments, plants were grown in parallel and wild type siblings were used as controls.

Stomatal phenotyping

Fully expanded leaf 3, 5, 7, and 10 were used for glue impression (Allsman, Dieffenbacher, and Rasmussen 2019) and prepared for the phenotyping slide. These slides were observed for stomatal phenotype using Nikon SMZ800N attached with ED plan 2X WF WD:35 objective lens and coupled with AmScope camera MU1003.

Stomatal conductance measurement

Stomatal conductance measurements were performed using CIRAS3 Portable Photo-Synthesis System. The leaf cuvette will maintain a stable environment: CO_2 concentration is 410 µmol mol^{-1}; H_20 reference is 80%; the cuvette flow is 300 cc min^{-1}. For all the measurements, healthy and fully expanded leaf 3 were used. Briefly, the leaf cuvette clamped the leaf and waited at least 30 mins to stabilize the initial stomatal conductance under the light (1000 PPFD). Lights were turned off immediately after the

initial conductance became stable, and the system recorded the transpirational conductance of the leaf surface simultaneously for the whole period of treatment. The data presented are the mean ± SE of at least 4 individual plants. Relative gs was computed for each individual measured plant by normalizing gs to the steady initial gs value observed. Data analysis was performed in R and JMP® 16.1.

Molecular cloning

Coding sequences of MLKS2 (primer pair: AA106 and AA107) and mNeonGreen (primer pair: AA108 and AA109) were amplified from *Zea mays* B73 cDNA and mNeonGreen-2A-mTurquoise2 (Addgene #98885), respectively. These amplified fragments are Goldengate compatible for type IIs restriction enzyme *Aar I*. Both MLKS2 and mNeonGreen were assembled into pType IIs plasmid using GeneArt™ Type IIs Assembly Kit, *Aar I* (Thermo Fisher Scientific #A15916). MLKS2-mNeonGreen from the pType IIs vector was further amplified (primer pair: AA98 and AA47) using attB1 and attB2 sites containing primers. This amplified product was first cloned into the entry vector pDONR221 using Gateway™ BP Clonase™ II Enzyme mix (Thermo Fisher Scientific #11789020) and eventually into the binary vector pMDC32 (ABRC #CD3-738) using Gateway™ LR Clonase™ II Enzyme mix (Thermo Fisher Scientific #11791020). Each cloned plasmids were confirmed by both restriction enzyme digestion and Sanger sequencing.

Transient expression and mitotic induction in *Nicotiana benthamiana*

For transient expression in *Nicotiana benthamiana, Agrobacterium* strain GV3101 harboring different constructs were resuspended in infiltration buffer (10 mM MES pH 5.7), 10 mM $MgCl_2$, 50 mg/L acetosyringone), and adjusted OD600 to 1.0. Equal volumes of cultures containing different constructs were mixed for co-infiltration. The resulting cultures were infiltrated into leaves of 3- to 4-week-old *Nicotiana benthamiana* plants. Leaf samples were imaged 48 hours after infiltration.

For motitic induction, equal volumes of cultures containing different constructs (pCaMV35S::ZmMLKS2-mNeonGreen and pCaMV35S::AtCYCD3;1) were mixed for co-infiltration. Leaf samples were imaged 48 hours after infiltration.

Confocal microscopy

Plant tissues were observed using a custom-built spinning disc confocal unit (3i) equipped with an inverted fluorescence microscope (IX83-ZDC, Olympus) CSU-W1 spinning disc with 50 micron pinholes (Yokogawa), aMesa Illumination Enhancement 7

Field Flattening unit (3i), an Andor iXon Life 888 EMCCD camera and a UPLANSAPO ×60 Silicone Oil-immersion objective (NA = 1.20, Olympus) and 4 laser stack with TTL controller (3i). For CFP, YFP/mNeonGreen and RFP imaging of maize and tobacco plants, a 445/515/561 dichroic (Chroma) was used. All emission filters are from Semrock. A 445 nm laser line and 483/45 emission filter (CFP) or 514 nm laser and 542/27 emission filter (YFP/mNeonGreen) was used.

Time-lapse imaging

For the time-lapse imaging, leaf meristematic regions of leaf 4 of corresponding plants were dissected and mounted with water. Cell division events were captured every 2 minutes with the spinning disk confocal microscope at Facette lab (details mentioned in the confocal microscopy section) for several hours.

Generation and purification of MLKS2 specific antibody

Two peptides corresponding to amino acids 10 to 24 (RQELDNLDKDADSRR) and 454 to 474 (SISRDKTPSPRASDRPINIDD) of maize MLKS2 were synthesized, co-injected into two separate rabbits and used for polyclonal antibody production in rabbits by Pacific Immunology (Ramona, CA) and named as MLKS2-17143 and MLKS2-17144. The resulting serum was affinity purified against the peptide using columns provided by Pacific Immunology. Affinity purified antibodies were eluted using Gentle Ag/Ab buffer (Pierce), desalted against TBS Buffer, and concentrated to 1 mg/ml using a 30K MWCO concentrator (Pierce).

Western blotting

Protein extraction for western blotting was performed as described previously (Facette et al. 2015). Briefly, 10-14 day old plants were used to isolate the basal 0.5-2.5 cm of unexpanded leaves 4-6, the leaf bases were ground in liquid nitrogen. Membrane fractions of extracts from these tissues were prepared. For western blotting, ~0.5 grams (3-5 plants) of tissue was used. Per 0.25 g of grounded tissue was mixed with 1ml extraction buffer (50mM Tris, pH 7.5, 150 mM NaCl, 5mM EGTA, 5mM EDTA 0.3% β-mercaptoethanol, 1% Sigma Plant Protease Inhibitor), the mixture was homogenized for 10s using an Omnitip homogenizer on ice. All subsequent steps were conducted at 4°C. The mixture was centrifuged twice at 13000*xg*. The supernatant was pelleted at 110,000xg for 60 min. Solubilization buffer (50 mM Tris pH 7.5, 150 mM NaCl, 1% NP-40, 10% glycerol, 0.05% Sodium deoxycholate) was then added to the pellet. For western blotting, extracts from plants were separated via SDS-PAGE and analyzed using anti-ZmMLKS2 at 2μg/ml.

Image processing and quantification

Nuclear position (Figure 3), actin patch formation (Figure 4), and correlation between PPB placement and nuclear position (Figure 5) were quantified in this study. The quantification strategies are explained in the following sections.

Nuclear positioning quantification

RanGAP-YFP marks the nuclear envelope and was used as a tool to observe the position of the nucleus. Previous study suggested that actin patch/nuclear polarization happens at the developmental stage, when the GMC width is 6μm (Facette et al. 2015). Meristematic regions of L3 of both wild type and *mlks2-1* plants were used to image RanGAP-YFP and SMCs associated with GMC width 6μm or more were considered for the nuclear position quantification. As shown in Figure 3A, If the nucleus is perfectly localized with the polarized cell wall, it is considered as a “polarized” nucleus. If the nucleus is not perfectly polarized, but touches an adjacent cell wall of the polarized cell wall, then it is considered as an “offset” nucleus. Finally, if the nucleus is far away from both the polarized and adjacent cell wall, then it is considered as an “unpolarized” nucleus. Based on this explained and demonstrated nuclear positioning rule, we have categorized nucleus into: Polarized, Offset, and Unpolarized.

Actin patch quantification

ABD2-YFP marker line was utilized to observe actin and nucleus position. Previously, it has been demonstrated that actin patch forms at the developmental stage, when the GMC width is 6μm (Facette et al. 2015). For our quantification, we have considered SMCs adjacent with GMC width 5μm or more. First, the actin patch was quantified from both polarized cell wall and adjacent cell wall by drawing a straight line at ImageJ/Fiji (Figure 4B). Then the intensity values were converted into ratios (polarized/adjacent) for each cell. These calculated intensity ratios were plotted at the Y-axis of Figure 4C. During the actin patch quantification, nucleus positioning was considered from the same cell. For the nucleus position quantification, similar rules were applied as RanGAP-YFP (Figure 3A).

Correlation between PPB placement and nuclear position

To observe both nuclear position and PPB, we have used the CFP-TUB marker line. CFP-TUB clearly marks PPB and nucleus from midplane and cortical PPB ring from the cortex. Cells with PPB were only considered for this quantification. If a SMC contains the PPB, then nuclear position in the same cell is observed, based on the rule explained in the earlier sections (Figure 3A).

Image processing was performed using ImageJ/Fiji and Adobe Illustrator version 26.0 for only linear adjustments and preserving hard edges.

Statistical analysis

Statistical tests, p value, number of plant samples, and number of individual cells used for experiments and quantification are mentioned in the corresponding figure legends. Data acquisition was done in Microsoft Excel; plotting the data and statistical tests were performed using JMP® 16.1.

Accession numbers

Gene and protein sequences for maize and Arabidopsis can be found at MaizeGDB (www.maizegdb.org) and TAIR (https://www.arabidopsis.org/index.jsp), respectively. Accession numbers for maize Version 4.0/Version 5.0 of the B73 genome are: *Mlks2*: Zm00001d052955 / Zm00001eb034900; *Pan1*: Zm00001d031437 / Zm00001eb200470; *AtCYCD3*: At4g34160.

Acknowledgments

We would like to thank Hardeep Gumber (Florida State University) and Hank Bass (Florida State University) for their initial work on the maize LINC complex and providing seeds. Authors are grateful to Bo Liu (University of California Davis) for providing p35S::AtCYCD3;1 plasmid for the mitotic induction experiment. Erika Norris (Undergraduate student at Facette lab) counted aberrant cells from summer field samples.

Funding

This project is supported in part by NSF IOS- 1754665, USDA NIFA Hatch MAS00570, and UMass Amherst Start-up funding to MRF.

Declaration of interests

The authors declare no competing interests.

Figure legends

Figure 1. MLKS2 is required for asymmetric cell division. A, Timeline for cell polarity establishment and mitotic events during the formation of subsidiary cells. B, Subsidiary cell phenotypes of *mlks2-1* and *mlks2-2*. White and yellow arrow indicate the normal and aberrant subsidiary cells, respectively. Scale bar = 20 µm. C, Quantification of aberrant subsidiary cells of *mlks2-1* and *mlks2-2*. At least 200 cells are observed from each individual plant. Statistical test is performed based on Tukey's Honest Test. Groups labelled with the same letter are not statistically different from each other (alpha = 0.05).

Figure 2. MLKS2 localizes at the nuclear membrane and with mitotic apparatus. A, Transient tobacco expression of MLKS2-mNG; where MLKS2 localizes at the nuclear membrane. After mitotic induction with AtCYCD3;1, MLKS2 also localizes at PPB (B), phragmoplast and new cell plate (C); and completes the mitosis (D). White arrow indicates nuclear membrane specific localization. Yellow arrow indicates PPB (B), phragmoplast and new cell plate (C); and completion of the mitosis (D).

Figure 3. Nuclear position is impaired in *mlks2-1*. A, Nuclear polarization model (polarized, offset, and unpolarized) used for quantification. B, Visualization of nuclear position using RanGAP-YFP in wild type and *mlks2-1*. Double white arrow head indicates the width of GMC and colored arrows, corresponding to (A), highlight the nuclear positioning. C, Quantification of the nucleus based on the polarization category in (A). Cells with GMC width 6µm or more were used for the quantification. 3 individual plants from both wild type and *mlks2-1* mutant were used for the experiment. 123 (polarized: 99, offset: 21, unpolarized: 3) and 155 (polarized: 98, offset: 43, unpolarized: 14) cells from wild type and *mlks2-1*, respectively, were observed for the quantification. The total number of cells based on nuclear polarization in each genotype are statistically tested by the Fisher's Exact test. P value is 0.0004. ***P <0.001. Scale bar = 10 µm.

Figure 4. Actin patch formation remains unaltered in *mlks2-1*. A, Visualization of actin patch formation at the GMC-SMC interface, and nuclear position using ABD2-YFP in wild type and *mlks2-1*. Nuclear position is marked with the dashed circle, where the color corresponds to (B), for polarized, offset, and unpolarized nucleus. Scale bar = 10 µm. B, Actin patch quantification was based on comparing the intensities between polarized and adjacent cell walls. C, Actin intensity ratio (polarized/adjacent cell wall) in wild type and *mlks2-1* for three distinct categories of nuclear positioning. 3 individual plants of each genotype were used for the experiment. Cells with GMC width 5µm or more were used for the quantification. Total 270 (Polarized: 206, Offset: 48,

Unpolarized: 16) and 206 (Polarized: 126, Offset: 58, Unpolarized: 22) cells from wild type and *mlks2-1*, respectively, were observed for the quantification. D, Nuclear polarization index of wild type and *mlks2-1* (from representative images in A, using the quantification strategy in B). The total number of cells based on nuclear polarization in each genotype are statistically tested by the Fisher's Exact test. P value is 0.0021. **P <0.01.

Figure 5. Nuclear positioning defect leads to misplaced PPB. Wildtype siblings and *mlks2* SMCs expressing CFP-TUB. A, Observation of PPB formation from midplane and cortex in wild type and *mlks2-1*. White and yellow arrow indicate PPB from wild type and *mlks2-1*, respectively. Scale bar = 10 µm. B, Six possible cellular events combining PPB placement (correct/incorrect) with nuclear position (Polarized/Offset/Unpolarized). Percentage of cells observed for corresponding events are mentioned in percentage for both wild type and *mlks2-1*. 3 individual plants of each genotype were used for the experiment. Total 338 and 446 cells from wild type and *mlks2-1*, respectively, were observed for the quantification.

Figure 6. Mitotic apparatus follows the division site marked by PPB. A, Time lapse of asymmetric cell division during subsidiary cell formation in wild type (upper panel) and *mlks2-1* (bottom panel). Nucleus and microtubule were visualized using HIS-YFP (magenta) and CFP-TUB (green), respectively. Nuclear envelope breakdown is considered as the starting point and marked as 0 min. Time-lapse movies were captured in every 2 min interval. Representative images highlighting key cell division stages: PPB, NEBD, metaphase, anaphase, telophase, and cytokinesis were presented. B, Quantification of PPB placement (Perfectly placed PPB/Misplaced PPB), nuclear positioning (P-polarized; O-offset; U-unpolarized), and cell division orientation (Expected division plane/Misoriented division plane) from the time lapse observation.

Figure 7. Graphical model of outer nuclear membrane protein-mediated nuclear positioning and future division site determination. (Left) In wild type condition, nucleus polarizes based on the established cell polarity, perfect PPB placement, and the mitotic apparatus follows the division site marked by PPB until cytokinesis. (Right) In *mlks2-1*, nucleus fails to position according to the established cell polarity, misplaced or transverse PPB based on the impaired nuclear position, and the mitotic apparatus follows the division site marked by PPB until cytokinesis.

Supplemental Data

Supplemental Figure S1. MLKS2 is an outer nuclear membrane protein and part of the LINC complex.

Supplemental Figure S2. MLKS2 is required for proper interstomatal cell and guard mother cell division.

Supplemental Figure S3. Aberrant subsidiary cell frequency of *mlks2-1* varies based on growth condition.

Supplemental Figure S4. Stomatal conductance is not affected in *mlks2-1*.

Supplemental Figure S5. Earlier cell polarity markers remain the same in *mlks2-1*.

Supplemental Figure S6. Mitotic spindle angle is altered in the *mlks2-1*.

Supplemental Figure S7. Transverse PPB formation in the *pan1-ems*.

Supplemental Figure S8. Telophase and cytokinesis require longer time in *mlks2-1*.

Supplemental Table S1. Primers used in this study for genotyping and cloning.

Supplementary Movie Legends

Supplemental Movie S1. **MLKS2 localizes at the nuclear membrane and with phragmoplast and new cell plate.** Transient tobacco expression with pCaMV35S::MLKS2-mNG and pCaMV35S::AtCYCD3. Time lapse movie was captured after 48h of the transformation. The images were captured in every 2 min interval.

Supplemental Movie S2. Asymmetric cell division of a SMC in a wild type plant. HIS-YFP (magenta) and CFP-TUB (green) were used for the visualization of nucleus and microtubules, respectively. The images were captured in every 2 min interval.

Supplemental Movie S3. Asymmetric cell division of a SMC in a *mlks2-1* cell. Transverse PPB placement with an offset nucleus leads to aberrant asymmetric cell division in *mlks2-1*. HIS-YFP (magenta) and CFP-TUB (green) were used for the visualization of nucleus and microtubules, respectively. The images were captured in every 2 min interval.

Supplemental Movie S4. SMC with a polarized nucleus and correctly aligned PPB from a wild type plant. The nuclear position is stable after PPB formation. HIS-YFP (magenta) and CFP-TUB (green) were used for the visualization of nucleus and microtubules, respectively. The images were captured in every 2 min interval.

Supplemental Movie S5. SMC with an unpolarized nucleus and transverse PPB from a *mlks2* plant. The unpolarized nucleus is slightly offset towards the GMC, but then centers itself within the transverse PPB in mlks2-1 cell. HIS-YFP (magenta) and CFP-TUB (green) were used for the visualization of nucleus and microtubules, respectively. The images were captured in every 2 min interval.

Supplemental Movie S6. **SMC with an initially polarized nucleus and perfectly placed PPB, which moves away from its polarized position, from a mlks2-1 plant** CFP-TUB, as green, marks PPB and nucleus. PAN2-YFP, as magenta, localizes at the GMC-SMC interphase. The images were captured in every 2 min interval.

Supplemental Movie S7. **Nuclear movement in a wild type cell prior to PPB formation.** HIS-YFP (magenta) and CFP-TUB (green) were used for the visualization of nucleus and microtubules, respectively. The images were captured in every 2 min interval.

Supplemental Movie S8. Nuclear movement in a mlks2-1 cell prior to PPB formation. HIS-YFP (magenta) and CFP-TUB (green) were used for the visualization of nucleus and microtubules, respectively. The images were captured in every 2 min interval.

References:

Allsman, Lindy A., Raquel N. Dieffenbacher, and Carolyn G. Rasmussen. 2019. "Glue Impressions of Maize Leaves and Their Use in Classifying Mutants." *Bio-Protocol*, April, e3209–e3209.

Apostolakos, P, P Livanos, E Giannoutsou, E Panteris, and B Galatis. 2018. "The Intracellular and Intercellular Cross-Talk during Subsidiary Cell Formation in Zea Mays: Existing and Novel Components Orchestrating Cell Polarization and Asymmetric Division." *Annals of Botany* 122 (5): 679–96. https://doi.org/10.1093/aob/mcx193.

Ashraf, M. Arif, and Michelle Facette. 2020. "Plant Biology: BASL Gives the Plant Nucleus a Sense of Direction." *Current Biology* 30 (22): R1375–77. https://doi.org/10.1016/j.cub.2020.09.009.

Barro, Amaya Vilches, Dorothee Stöckle, Martha Thellmann, Paola Ruiz-Duarte, Lotte Bald, Marion Louveaux, Patrick von Born, Philipp Denninger, Tatsuaki Goh, and Hidehiro Fukaki. 2019. "Cytoskeleton Dynamics Are Necessary for Early Events of Lateral Root Initiation in Arabidopsis." *Current Biology* 29 (15): 2443–54.

Best, Norman B, Charles Addo-Quaye, Bong-Suk Kim, Clifford F Weil, Burkhard Schulz, Guri Johal, and Brian P Dilkes. 2021. "Mutation of the Nuclear Pore Complex Component, Aladin1, Disrupts Asymmetric Cell Division in Zea Mays (Maize)." *G3 Genes*|*Genomes*|*Genetics* 11 (7): jkab106. https://doi.org/10.1093/g3journal/jkab106.

Brueggeman, Justin M, Ian A Windham, and Andreas Nebenführ. 2022. "Nuclear Movement in Growing Arabidopsis Root Hairs Involves Both Actin Filaments and Microtubules." *Journal of Experimental Botany*, May, erac207. https://doi.org/10.1093/jxb/erac207.

Buschmann, Henrik, and Sabine Zachgo. 2016. "The Evolution of Cell Division: From Streptophyte Algae to Land Plants." *Trends in Plant Science* 21 (10): 872–83. https://doi.org/10.1016/j.tplants.2016.07.004.

Cartwright, Heather N., John A. Humphries, and Laurie G. Smith. 2009. "A Receptor-Like Protein That Promotes Polarization of an Asymmetric Cell Division in Maize." *Science* 323 (5914): 649–51. https://doi.org/10.1126/science.1161686.

Facette, Michelle R., Yeri Park, Dena Sutimantanapi, Anding Luo, Heather N. Cartwright, Bing Yang, Eric J. Bennett, Anne W. Sylvester, and Laurie G. Smith. 2015. "The SCAR/WAVE Complex Polarizes PAN Receptors and Promotes Division Asymmetry in Maize." *Nature Plants* 1 (2): 1–8. https://doi.org/10.1038/nplants.2014.24.

Facette, Michelle R, Carolyn G Rasmussen, and Jaimie M Van Norman. 2019. "A Plane Choice: Coordinating Timing and Orientation of Cell Division during Plant Development." *Current Opinion in Plant Biology*, Growth and development, 47 (February): 47–55. https://doi.org/10.1016/j.pbi.2018.09.001.

Fal, Kateryna, Atef Asnacios, Marie-Edith Chabouté, and Olivier Hamant. 2017. "Nuclear Envelope: A New Frontier in Plant Mechanosensing?" *Biophysical Reviews* 9 (4): 389–403. https://doi.org/10.1007/s12551-017-0302-6.

Gallagher, Kimberly, and Laurie G. Smith. 2000. "Roles for Polarity and Nuclear Determinants in Specifying Daughter Cell Fates after an Asymmetric Cell Division in the Maize Leaf." *Current Biology* 10 (19): 1229–32. https://doi.org/10.1016/S0960-9822(00)00730-2.

Graumann, Katja, and David E. Evans. 2011. "Nuclear Envelope Dynamics during Plant Cell Division Suggest Common Mechanisms between Kingdoms." *Biochemical Journal* 435 (3): 661–67. https://doi.org/10.1042/BJ20101769.

Groves, Norman Reid, Alecia Biel, Morgan Moser, Tyler Mendes, Katelyn Amstutz, and Iris Meier. 2020. "Recent Advances in Understanding the Biological Roles of the Plant Nuclear Envelope." *Nucleus* 11 (1): 330–46. https://doi.org/10.1080/19491034.2020.1846836.

Gumber, Hardeep K., Joseph F. McKenna, Amado L. Estrada, Andrea F. Tolmie, Katja Graumann, and Hank W. Bass. 2019. "Identification and Characterization of Genes Encoding the Nuclear Envelope LINC Complex in the Monocot Species Zea Mays." *Journal of Cell Science* 132 (3): jcs221390. https://doi.org/10.1242/jcs.221390.

Gumber, Hardeep K., Joseph F. McKenna, Andrea F. Tolmie, Alexis M. Jalovec, Andre C. Kartick, Katja Graumann, and Hank W. Bass. 2019. "MLKS2 Is an ARM Domain and F-Actin-Associated KASH Protein That Functions in Stomatal Complex Development and Meiotic Chromosome Segregation." *Nucleus* 10 (1): 144–66. https://doi.org/10.1080/19491034.2019.1629795.

Humphries, John A., Zuzana Vejlupkova, Anding Luo, Robert B. Meeley, Anne W. Sylvester, John E. Fowler, and Laurie G. Smith. 2011. "ROP GTPases Act with the Receptor-Like Protein PAN1 to Polarize Asymmetric Cell Division in Maize." *The Plant Cell* 23 (6): 2273–84. https://doi.org/10.1105/tpc.111.085597.

Kawashima, Tomokazu, Daisuke Maruyama, Murat Shagirov, Jing Li, Yuki Hamamura, Ramesh Yelagandula, Yusuke Toyama, and Frédéric Berger. 2014. "Dynamic F-Actin Movement Is Essential for Fertilization in Arabidopsis Thaliana." *Elife* 3: e04501.

Kennard, Janelle L., and Ann L. Cleary. 1997. "Pre-Mitotic Nuclear Migration in Subsidiary Mother Cells of Tradescantia Occurs in G1 of the Cell Cycle and Requires F-Actin." *Cell Motility* 36 (1): 55–67. https://doi.org/10.1002/(SICI)1097-0169(1997)36:1<55::AID-CM5>3.0.CO;2-G.

Kimata, Yusuke, Takumi Higaki, Tomokazu Kawashima, Daisuke Kurihara, Yoshikatsu Sato, Tomomi Yamada, Seiichiro Hasezawa, Frederic Berger, Tetsuya Higashiyama, and Minako Ueda. 2016. "Cytoskeleton Dynamics Control the First Asymmetric Cell Division in Arabidopsis Zygote." *Proceedings of the National Academy of Sciences* 113 (49): 14157–62. https://doi.org/10.1073/pnas.1613979113.

Kimata, Yusuke, Takehide Kato, Takumi Higaki, Daisuke Kurihara, Tomomi Yamada, Shoji Segami, Miyo Terao Morita, Masayoshi Maeshima, Seiichiro Hasezawa, and Tetsuya Higashiyama. 2019. "Polar Vacuolar Distribution Is Essential for Accurate Asymmetric Division of Arabidopsis Zygotes." *Proceedings of the*

National Academy of Sciences 116 (6): 2338–43.

Krishnakumar, Vivek, Yongwook Choi, Erin Beck, Qingyu Wu, Anding Luo, Anne Sylvester, David Jackson, and Agnes P. Chan. 2015. "A Maize Database Resource That Captures Tissue-Specific and Subcellular-Localized Gene Expression, via Fluorescent Tags and Confocal Imaging (Maize Cell Genomics Database)." *Plant and Cell Physiology* 56 (1): e12. https://doi.org/10.1093/pcp/pcu178.

Li, Rong. 2013. "The Art of Choreographing Asymmetric Cell Division." *Developmental Cell* 25 (5): 439–50. https://doi.org/10.1016/j.devcel.2013.05.003.

Livanos, Pantelis, and Sabine Müller. 2019. "Division Plane Establishment and Cytokinesis." *Annual Review of Plant Biology* 70 (April): 239–67. https://doi.org/10.1146/annurev-arplant-050718-100444.

Martinez, Pablo, Lindy A. Allsman, Kenneth A. Brakke, Christopher Hoyt, Jordan Hayes, Hong Liang, Wesley Neher, et al. 2018. "Predicting Division Planes of Three-Dimensional Cells by Soap-Film Minimization." *The Plant Cell* 30 (10): 2255–66. https://doi.org/10.1105/tpc.18.00401.

Martinez, Pablo, Anding Luo, Anne Sylvester, and Carolyn G. Rasmussen. 2017. "Proper Division Plane Orientation and Mitotic Progression Together Allow Normal Growth of Maize." *Proceedings of the National Academy of Sciences* 114 (10): 2759–64. https://doi.org/10.1073/pnas.1619252114.

Miki, Tomohiro, Haruko Naito, Momoko Nishina, and Gohta Goshima. 2014. "Endogenous Localizome Identifies 43 Mitotic Kinesins in a Plant Cell." *Proceedings of the National Academy of Sciences* 111 (11): E1053–61. https://doi.org/10.1073/pnas.1311243111.

Mohanty, Amitabh, Anding Luo, Stacy DeBlasio, Xingyuan Ling, Yan Yang, Dorothy E. Tuthill, Katherine E. Williams, et al. 2009. "Advancing Cell Biology and Functional Genomics in Maize Using Fluorescent Protein-Tagged Lines." *Plant Physiology* 149 (2): 601–5. https://doi.org/10.1104/pp.108.130146.

Moukhtar, Julien, Alain Trubuil, Katia Belcram, David Legland, Zhor Khadir, Aurélie Urbain, Jean-Christophe Palauqui, and Philippe Andrey. 2019. "Cell Geometry Determines Symmetric and Asymmetric Division Plane Selection in Arabidopsis Early Embryos." *PLOS Computational Biology* 15 (2): e1006771. https://doi.org/10.1371/journal.pcbi.1006771.

Murata, Takashi, and Masamitsu Wada. 1991. "Effects of Centrifugation on Preprophase-Band Formation in Adiantum Protonemata." *Planta* 183 (3): 391–98. https://doi.org/10.1007/BF00197738.

Muroyama, Andrew, Yan Gong, and Dominique C. Bergmann. 2020. "Opposing, Polarity-Driven Nuclear Migrations Underpin Asymmetric Divisions to Pattern Arabidopsis Stomata." *Current Biology* 30 (22): 4467–75.

Oda, Yoshihisa, and Hiroo Fukuda. 2011. "Dynamics of Arabidopsis SUN Proteins during Mitosis and Their Involvement in Nuclear Shaping." *The Plant Journal* 66 (4): 629–41. https://doi.org/10.1111/j.1365-313X.2011.04523.x.

Panteris, Emmanuel, Panagiotis Apostolakos, and Basil Galatis. 2006. "Cytoskeletal Asymmetry in Zea Mays Subsidiary Cell Mother Cells: A Monopolar Prophase Microtubule Half-Spindle Anchors the Nucleus to Its Polar Position." *Cell Motility and the Cytoskeleton* 63 (11): 696–709.

Raissig, Michael T., Juliana L. Matos, M. Ximena Anleu Gil, Ari Kornfeld, Akhila Bettadapur, Emily Abrash, Hannah R. Allison, et al. 2017. "Mobile MUTE Specifies Subsidiary Cells to Build Physiologically Improved Grass Stomata." *Science* 355 (6330): 1215–18. https://doi.org/10.1126/science.aal3254.

Rasmussen, Carolyn G., and Marschal Bellinger. 2018. "An Overview of Plant Division-Plane Orientation." *New Phytologist* 219 (2): 505–12. https://doi.org/10.1111/nph.15183.

Schaefer, Estelle, Katia Belcram, Magalie Uyttewaal, Yann Duroc, Magali Goussot, David Legland, Elise Laruelle, Marie-Ludivine de Tauzia-Moreau, Martine Pastuglia, and David Bouchez. 2017. "The Preprophase Band of Microtubules Controls the Robustness of Division Orientation in Plants." *Science* 356 (6334): 186–89. https://doi.org/10.1126/science.aal3016.

Tapley, Erin C, and Daniel A Starr. 2013. "Connecting the Nucleus to the Cytoskeleton by SUN–KASH Bridges across the Nuclear Envelope." *Current Opinion in Cell Biology*, Cell architecture, 25 (1): 57–62. https://doi.org/10.1016/j.ceb.2012.10.014.

Uzer, Gunes, Clinton T. Rubin, and Janet Rubin. 2016. "Cell Mechanosensitivity Is Enabled by the LINC Nuclear Complex." *Current Molecular Biology Reports* 2 (1): 36–47. https://doi.org/10.1007/s40610-016-0032-8.

Xu, Jie, Yuh-Ru Julie Lee, and Bo Liu. 2020. "Establishment of a Mitotic Model System by Transient Expression of the D-Type Cyclin in Differentiated Leaf Cells of Tobacco (Nicotiana Benthamiana)." *New Phytologist* 226 (4): 1213–20. https://doi.org/10.1111/nph.16309.

Yi, Peishan, and Gohta Goshima. 2020. "Rho of Plants GTPases and Cytoskeletal Elements Control Nuclear Positioning and Asymmetric Cell Division during Physcomitrella Patens Branching." *Current Biology* 30 (14): 2860–68.

Yi, Peishan, and Gohta Goshima. 2022. "Division Site Determination during Asymmetric Cell Division in Plants." *The Plant Cell* 34 (6): 2120–39. https://doi.org/10.1093/plcell/koac069.

Zhang, Dan, Emily B. Abrash, Tiago D. G. Nunes, Ines Hidalgo Prados, M. Ximena Anleu Gil, Barbara Jesenofsky, Heike Lindner, Dominique C. Bergmann, and Michael T. Raissig. 2022. "Opposite Polarity Programs Regulate Asymmetric Subsidiary Cell Divisions in Grasses." bioRxiv. https://doi.org/10.1101/2022.04.24.489281.

Zhang, Xiaoguo, Michelle Facette, John A. Humphries, Zhouxin Shen, Yeri Park, Dena Sutimantanapi, Anne W. Sylvester, Steven P. Briggs, and Laurie G. Smith. 2012. "Identification of PAN2 by Quantitative Proteomics as a Leucine-Rich Repeat–Receptor-Like Kinase Acting Upstream of PAN1 to Polarize Cell Division in Maize." *The Plant Cell* 24 (11): 4577–89. https://doi.org/10.1105/tpc.112.104125.

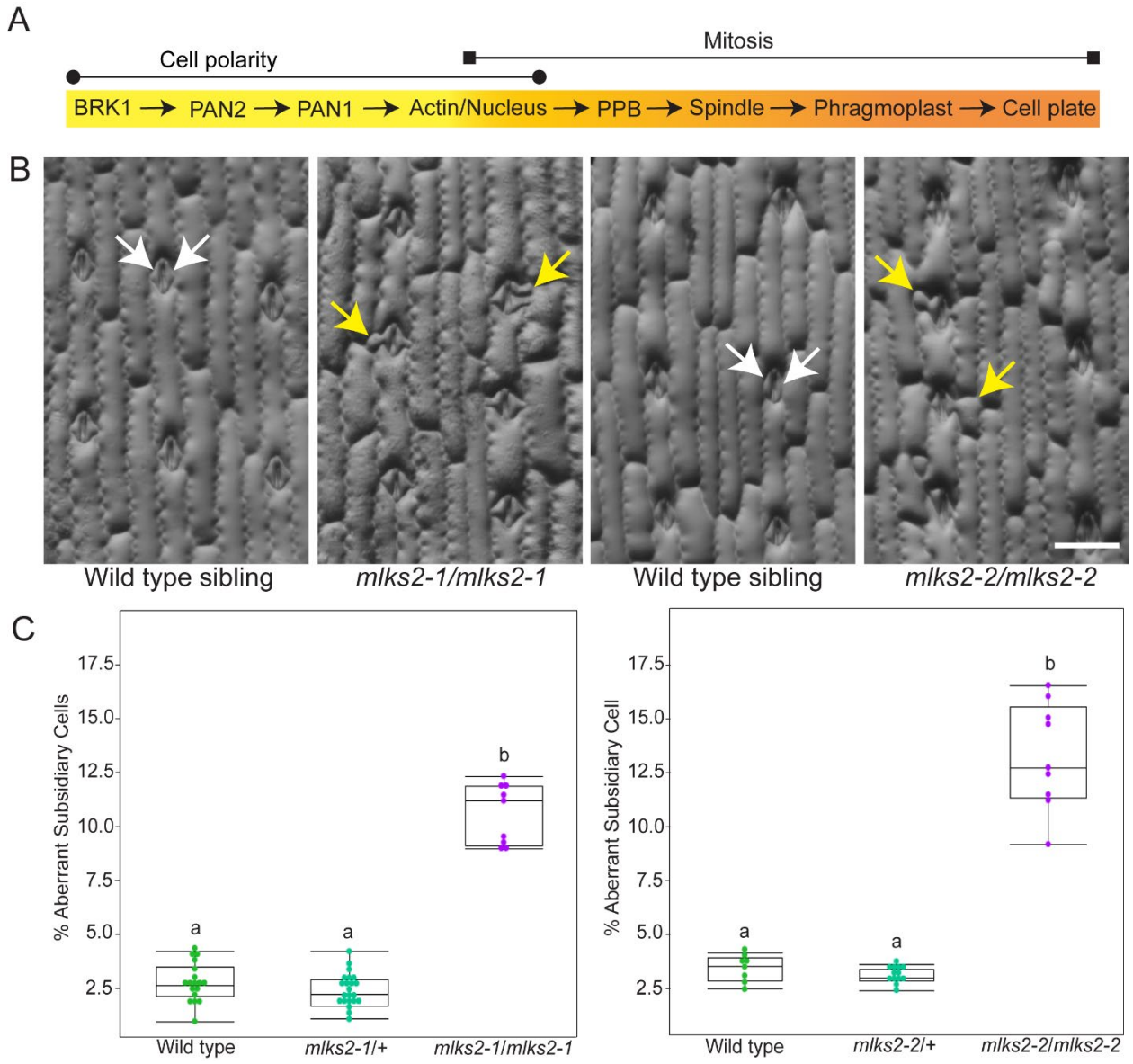

Figure 1. MLKS2 is required for asymmetric cell division. A, Timeline for cell polarity establishment and mitotic events during the formation of subsidiary cells. B, Subsidiary cell phenotypes of *mlks2-1* and *mlks2-2*. White and yellow arrow indicate the normal and aberrant subsidiary cells, respectively. Scale bar = 20 μm. C, Quantification of aberrant subsidiary cells of *mlks2-1* and *mlks2-2*. At least 200 cells are observed from each individual plant. Statistical test is performed based on Tukey's Honest Test. Groups labelled with the same letter are not statistically different from each other (alpha = 0.05).

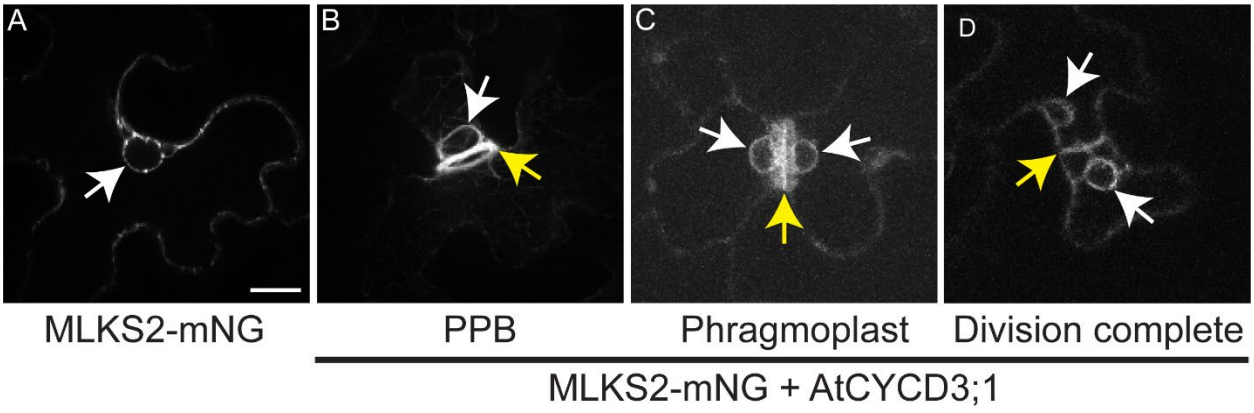

Figure 2. MLKS2 localizes at the nuclear membrane and with mitotic apparatus. A, Transient tobacco expression of MLKS2-mNG; where MLKS2 localizes at the nuclear membrane. After mitotic induction with AtCYCD3;1, MLKS2 also localizes at PPB (B), phragmoplast and new cell plate (C); and completes the mitosis (D). White arrow indicates nuclear membrane specific localization. Yellow arrow indicates PPB (B), phragmoplast and new cell plate (C); and completion of the mitosis (D). Scale bar = 20 µm.

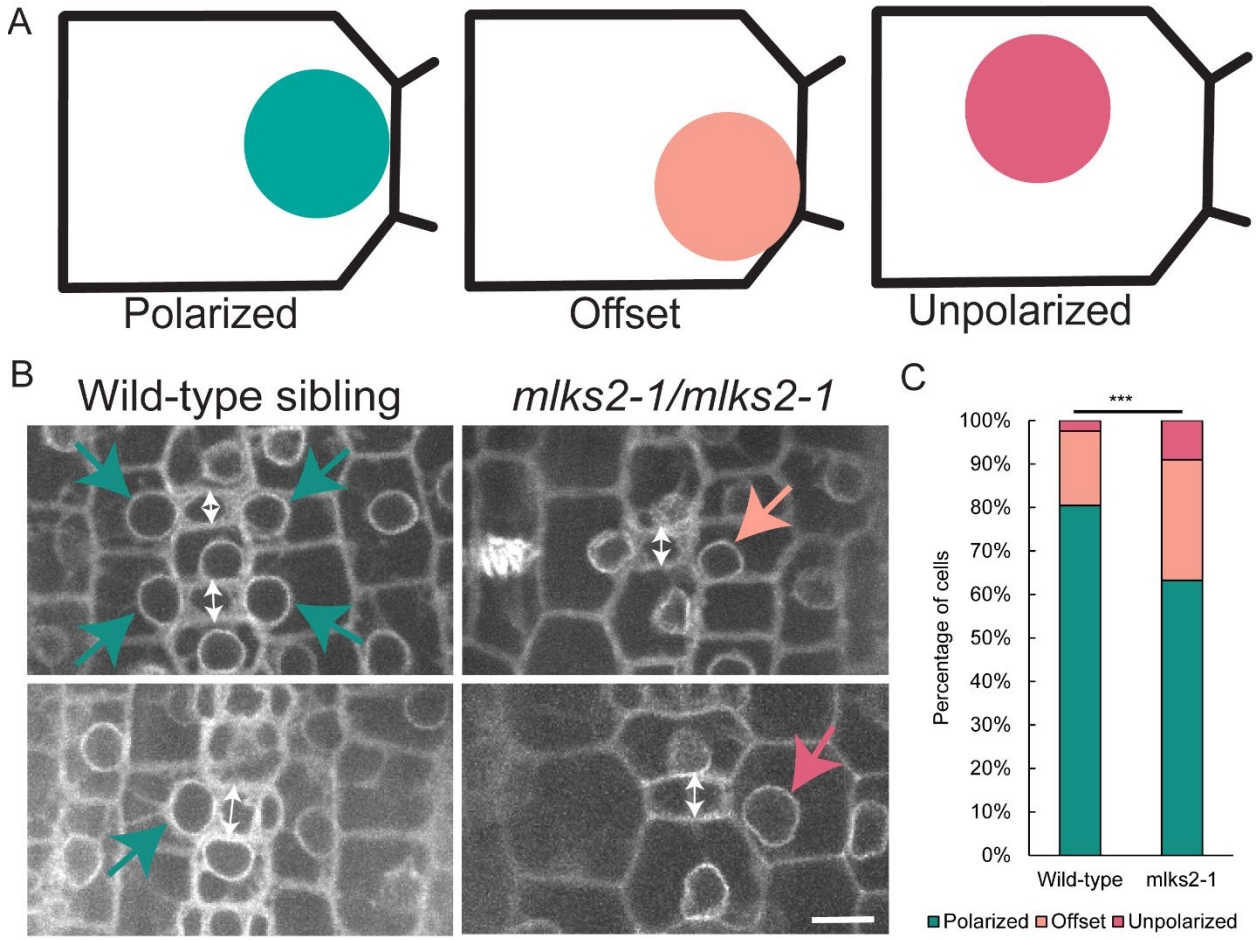

Figure 3. Nuclear position is impaired in *mlks2-1*. A, Nuclear polarization model (polarized, offset, and unpolarized) used for quantification. B, Visualization of nuclear position using RanGAP-YFP in wild type and *mlks2-1*. Double white arrow head indicates the width of GMC and colored arrows, corresponding to (A), highlight the nuclear positioning. C, Quantification of the nucleus based on the polarization category in (A). Cells with GMC width 6μm or more were used for the quantification. 3 individual plants from both wild type and *mlks2-1* mutant were used for the experiment. 123 (polarized: 99, offset: 21, unpolarized: 3) and 155 (polarized: 98, offset: 43, unpolarized: 14) cells from wild type and *mlks2-1*, respectively, were observed for the quantification. The total number of cells based on nuclear polarization in each genotype are statistically tested by the Fisher's Exact test. P value is 0.0004. ***P <0.001. Scale bar = 10 μm.

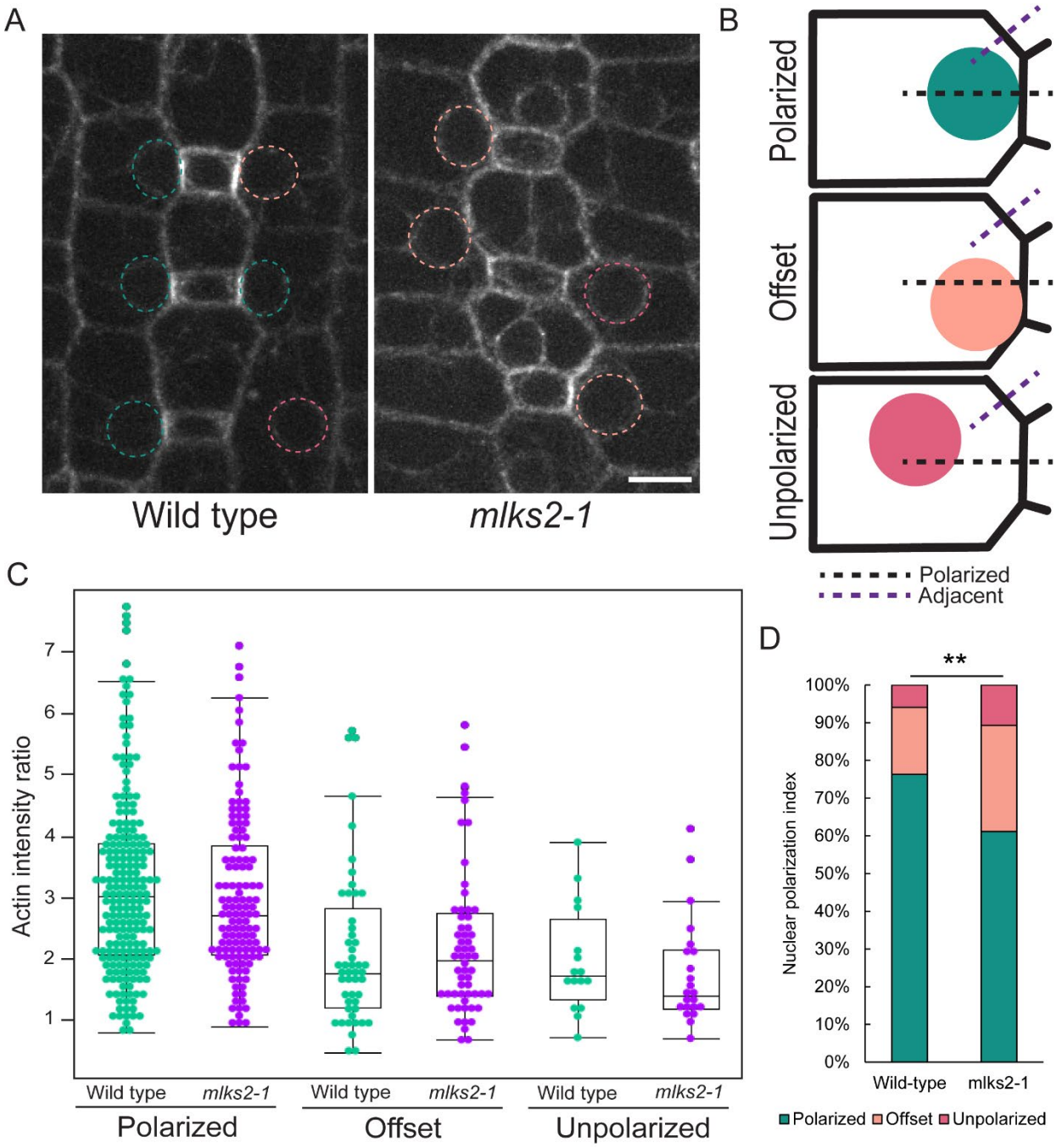

Figure 4. Actin patch formation remains unaltered in *mlks2-1*. A, Visualization of actin patch formation in the GMC-SMC interphase, as polarity marker, and nuclear position using ABD2-YFP in wild type and *mlks2-1*. Nuclear position is marked with the dashed circle, corresponding to (B), for polarized, offset, and unpolarized nucleus. Scale bar = 10 µm. B, Actin patch quantification was based on comparing the intensities

between polarized and adjacent cell walls. C, Actin intensity ratio (polarized/adjacent cell wall) in wild type and *mlks2-1* for three distinct categories of nuclear positioning. 3 individual plants of each genotype were used for the experiment. Cells with GMC width 5μm or more were used for the quantification. Total 270 (Polarized: 206, Offset: 48, Unpolarized: 16) and 206 (Polarized: 126, Offset: 58, Unpolarized: 22) cells from wild type and *mlks2-1*, respectively, were observed for the quantification. D, Nuclear polarization index of wild type and *mlks2-1* (from representative images in A, using the quantification strategy in B). The total number of cells based on nuclear polarization in each genotype are statistically tested by the Fisher's Exact test. P value is 0.0021. **P <0.01.

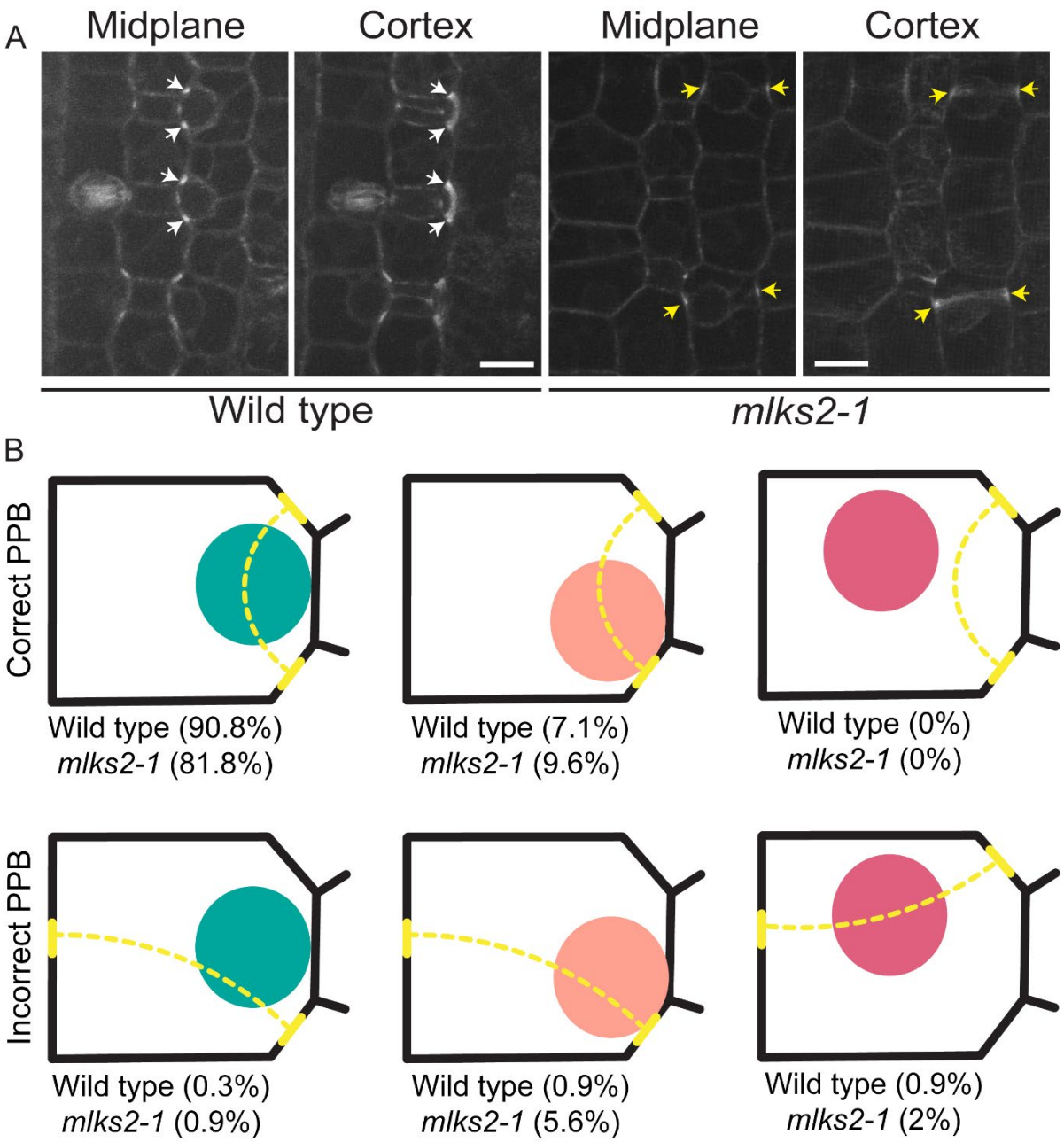

Figure 5. Nuclear positioning defect leads to misplaced PPB. A, Observation of PPB formation from midplane and cortex using CFP-TUB in wild type and *mlks2-1*. White and yellow arrow indicate PPB from wild type and *mlks2-1*, respectively. Scale bar = 10 µm. B, Six probable cellular events combining PPB placement (correct/incorrect) with nuclear position (Polarized/Offset/Unpolarized). Percentage of cells observed for corresponding events are mentioned in percentage for both wild type and *mlks2-1*. 3 individual plants of each genotype were used for the experiment. Total 338 and 446 cells from wild type and *mlks2-1*, respectively, were observed for the quantification.

A

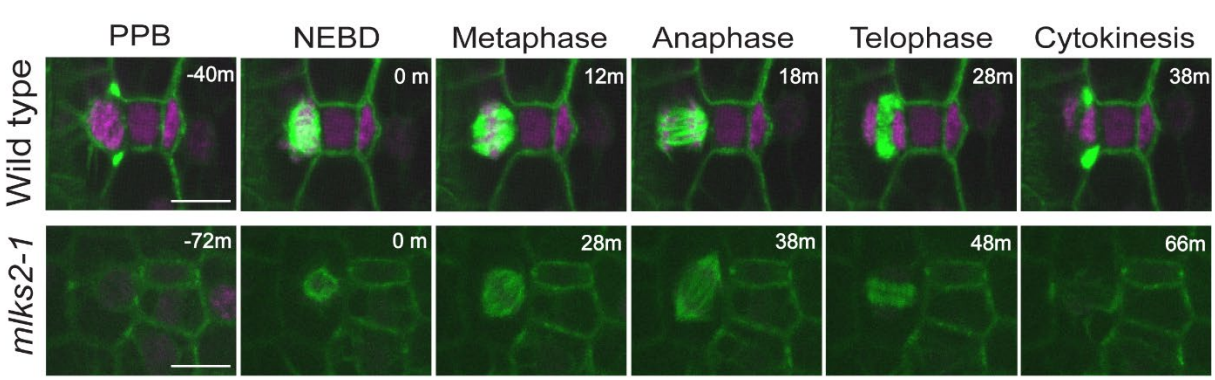

B

Wild type						*mlks2-1*					
Perfectly placed PPB			Misplaced PPB			Perfectly placed PPB			Misplaced PPB		
27			0			25			10		
P	O	U	P	O	U	P	O	U	P	O	U
26	1	0	0	0	0	25	0	0	0	6	4

Figure 6. Mitotic apparatus follows the division site marked by PPB. A, Time lapse of asymmetric cell division during subsidiary cell formation in wild type (upper panel) and *mlks2-1* (bottom panel). Nucleus and microtubule were visualized using HIS-YFP (magenta) and CFP-TUB (green), respectively. Nuclear envelope breakdown is considered as the starting point and marked as 0 min. Time lapse movies were captured in every 2 min interval. Representative images highlighting key cell division stages: PPB, NEBD, metaphase, anaphase, telophase, and cytokinesis were presented. Scale bar = 10 μm. B, Quantification of PPB placement (Perfectly placed PPB/Misplaced PPB), nuclear positioning (P-polarized; O-offset; U-unpolarized), and cell division orientation (Expected division plane/Misoriented division plane) from the time lapse observation.

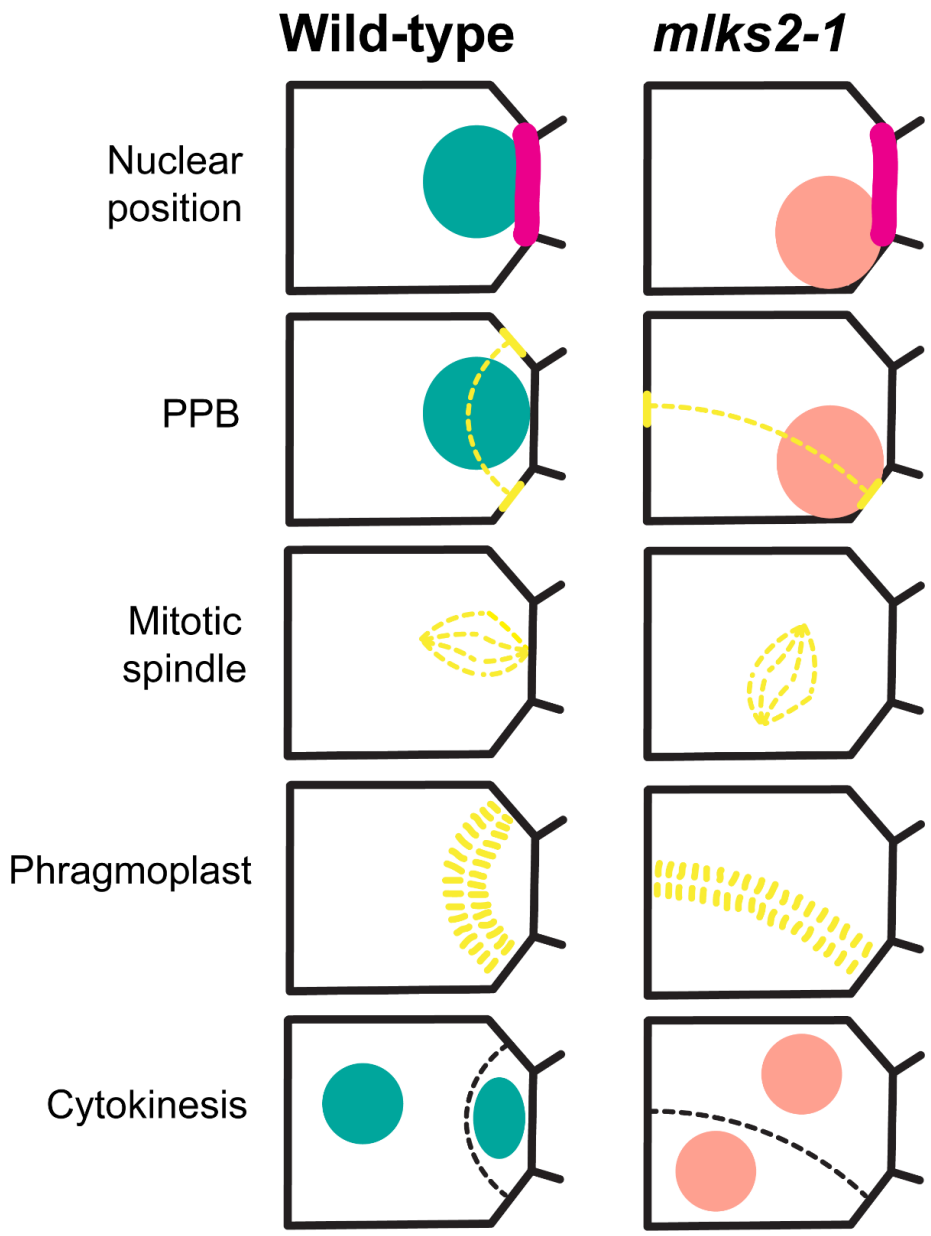

Figure 7. Graphical model of outer nuclear membrane protein-mediated nuclear positioning and future division site determination. (Left) In wild type condition, nucleus polarizes based on the established cell polarity, perfect PPB placement, and the mitotic apparatus follows the division site marked by PPB until cytokinesis. (Right) In *mlks2-1*, nucleus fails to position according to the established cell polarity, misplaced or transverse PPB based on the impaired nuclear position, and the mitotic apparatus follows the division site marked by PPB until cytokinesis.

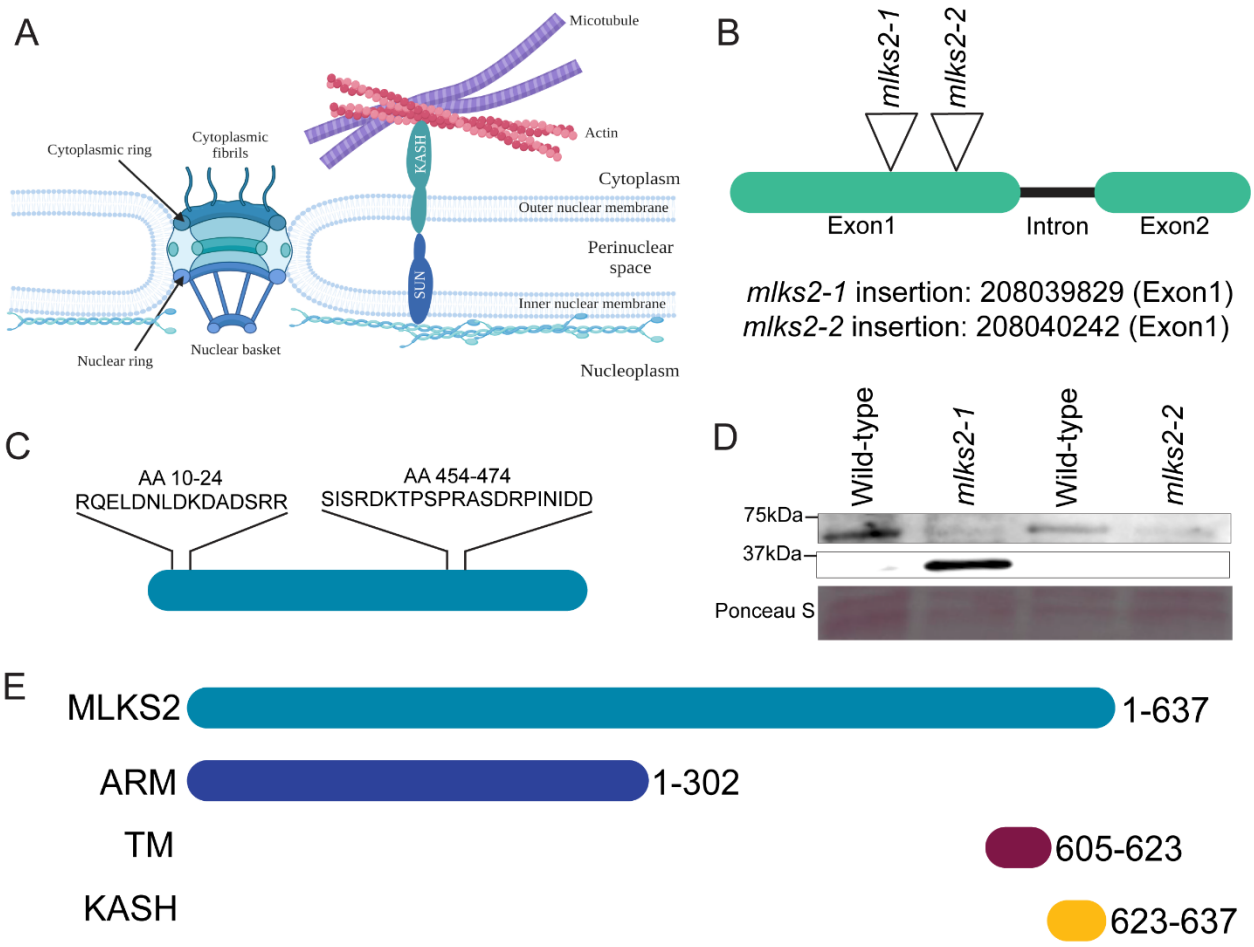

Supplemental Figure S1. MLKS2 is an outer nuclear membrane protein and part of the LINC complex. A, KASH-domain containing outer nuclear membrane protein interacts with SUN-domain containing inner nuclear membrane protein in the perinuclear space. KASH-domain containing outer nuclear membrane protein MLKS2 interacts with cytoskeleton. B, Position of two Mu insertion lines, *mlks2-1* and *mlks2-2*, of *Mlks2*. C, Target amino acid sequences used for the MLKS2 antibody production. D, Western blot of wild type, *mlks2-1*, *mlks2-2* using MLKS2 antibodies. Ponceau S staining indicates the protein loading control. E, Domain organization of MLKS2 protein: Armadillo domain (1-302 aa), transmembrane domain (605-623), and KASH domain (623-637).

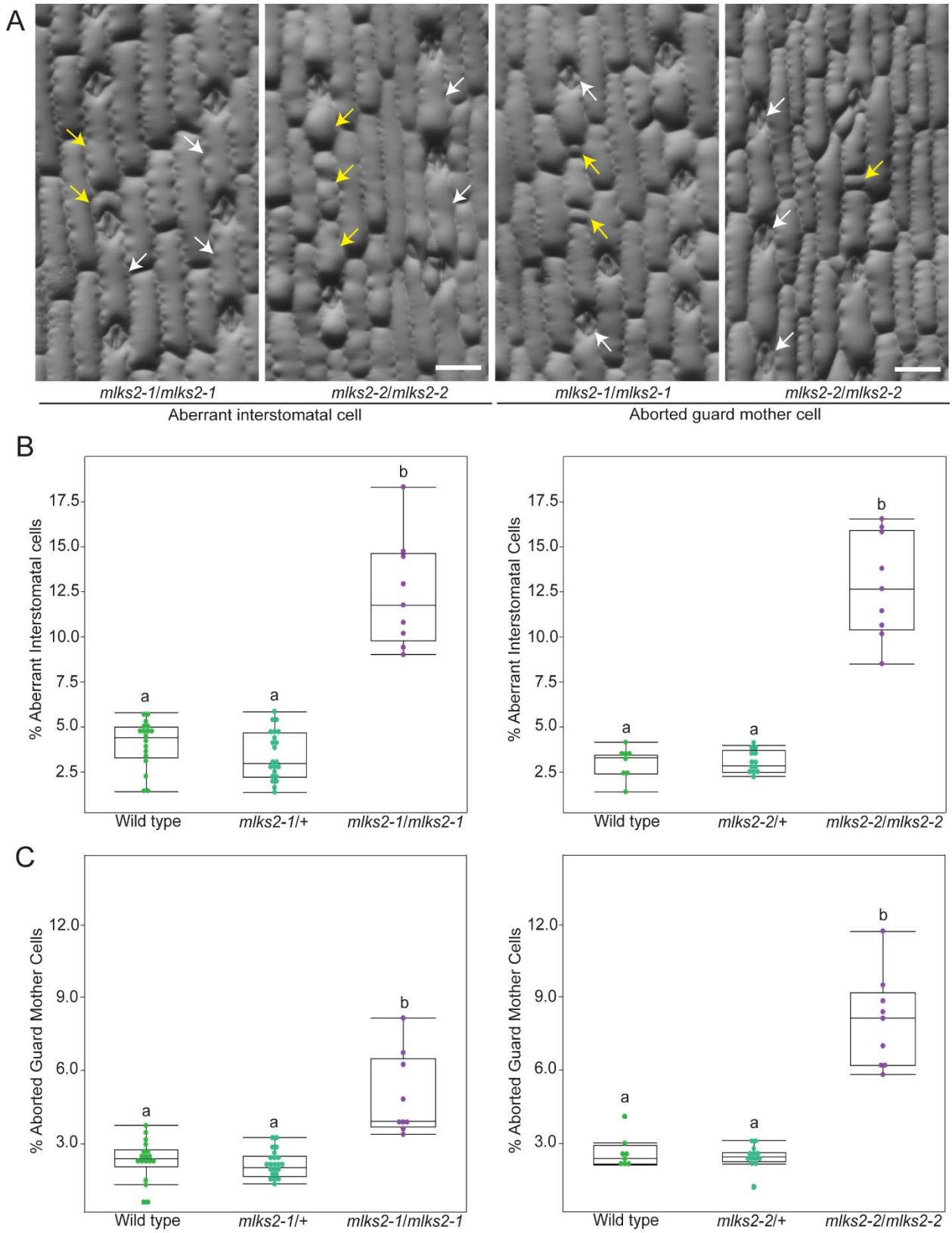
A
mlks2-1/mlks2-1
mlks2-2/mlks2-2
mlks2-1/mlks2-1
mlks2-2/mlks2-2
Aberrant interstomatal cell
Aborted guard mother cell
B
% Aberrant Interstomatal cells
% Aberrant Interstomatal Cells
17.5
15.0
12.5
10.0
7.5
5.0
2.5
a
a
b
Wild type
mlks2-1/+
mlks2-1/mlks2-1
mlks2-2/+
mlks2-2/mlks2-2
C
% Aborted Guard Mother Cells
12.0
9.0
6.0
3.0

Supplemental Figure S2. MLKS2 is required for proper interstomatal cell and guard cell division. A, Interstomatal cell and aborted guard mother cell phenotypes of *mlks2-1* and *mlks2-2*. White and yellow arrow indicate the normal and aberrant interstomatal cell or aborted guard mother cell, respectively. Scale bar = 20 μm. B, Quantification of aberrant interstomatal cell of *mlks2-1* and *mlks2-2*. C, Quantification of aborted guard mother cells of *mlks2-1* and *mlks2-2*. At least 200 cells are observed from each individual plant. Statistical test is performed based on Tukey's Honest Test. Groups labelled with the same letter are not statistically different from each other (alpha = 0.05).

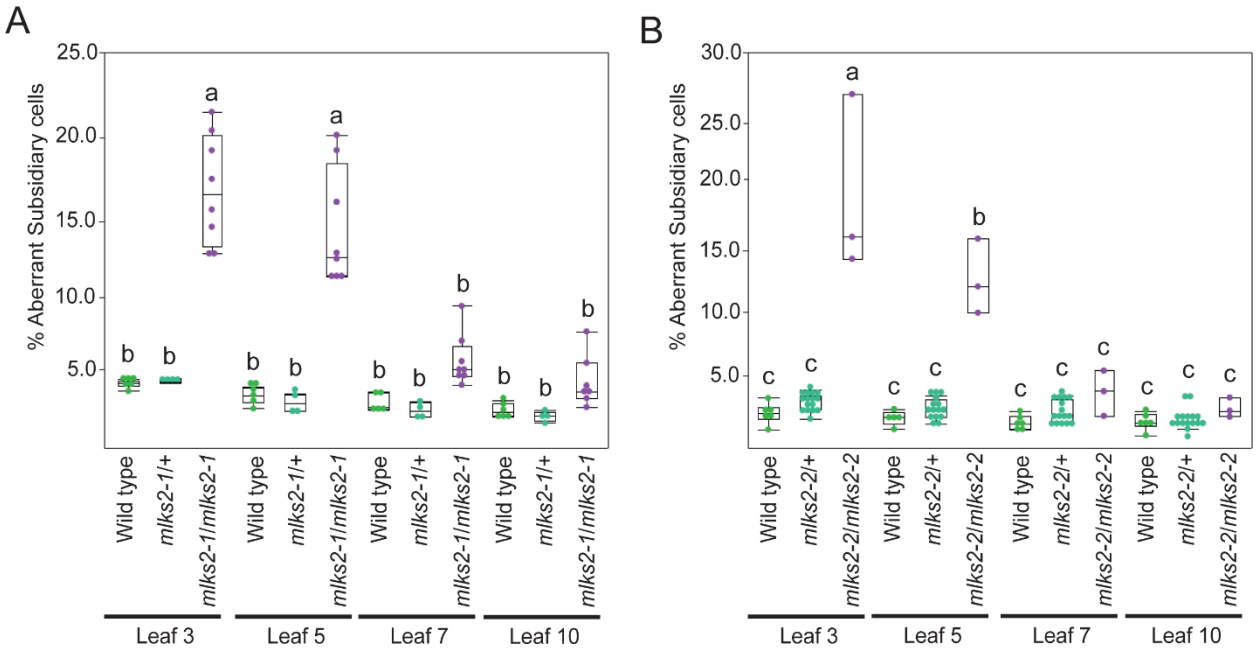

Supplemental Figure S3. Aberrant subsidiary cell frequency of *mlks2-1* varies based on growth condition. Quantification of aberrant subsidiary cells from leaf 3, 5, 7, and 10 of *mlks2-1* (A) and *mlks2-2* (B) grown in the summer field. At least 200 cells are observed from each individual plant. Statistical test is performed based on Tukey's Honest Test. Groups labelled with the same letter are not statistically different from each other (alpha = 0.05).

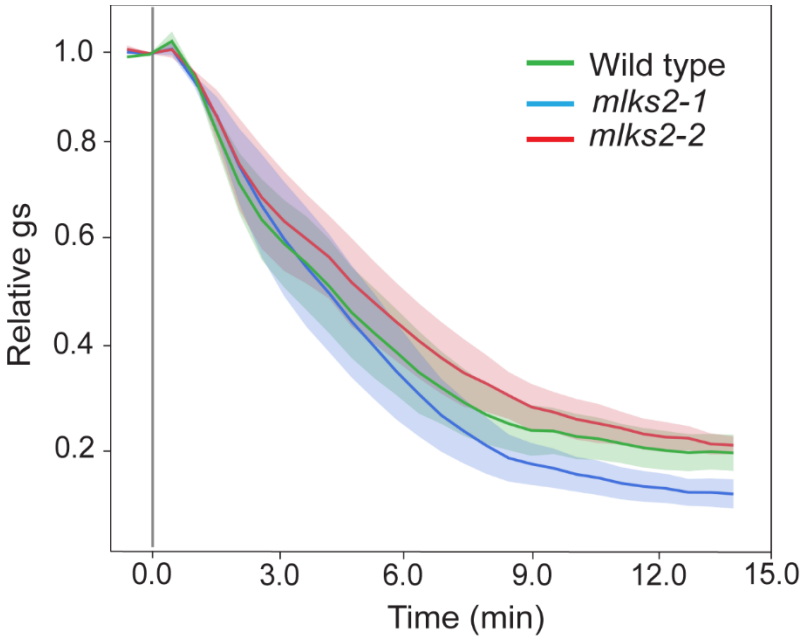

Supplemental Figure S4. Stomatal conductance is not affected in *mlks2-1*. Stomatal conductance of *mlks2-1* and *mlks2-2* were measured using the CIRAS3 Portable Photo-Synthesis System. The data presented are the mean ± SE of at least 4 individual plants. Relative gs was computed for each individual measured plant by normalizing gs to the steady initial gs value observed.

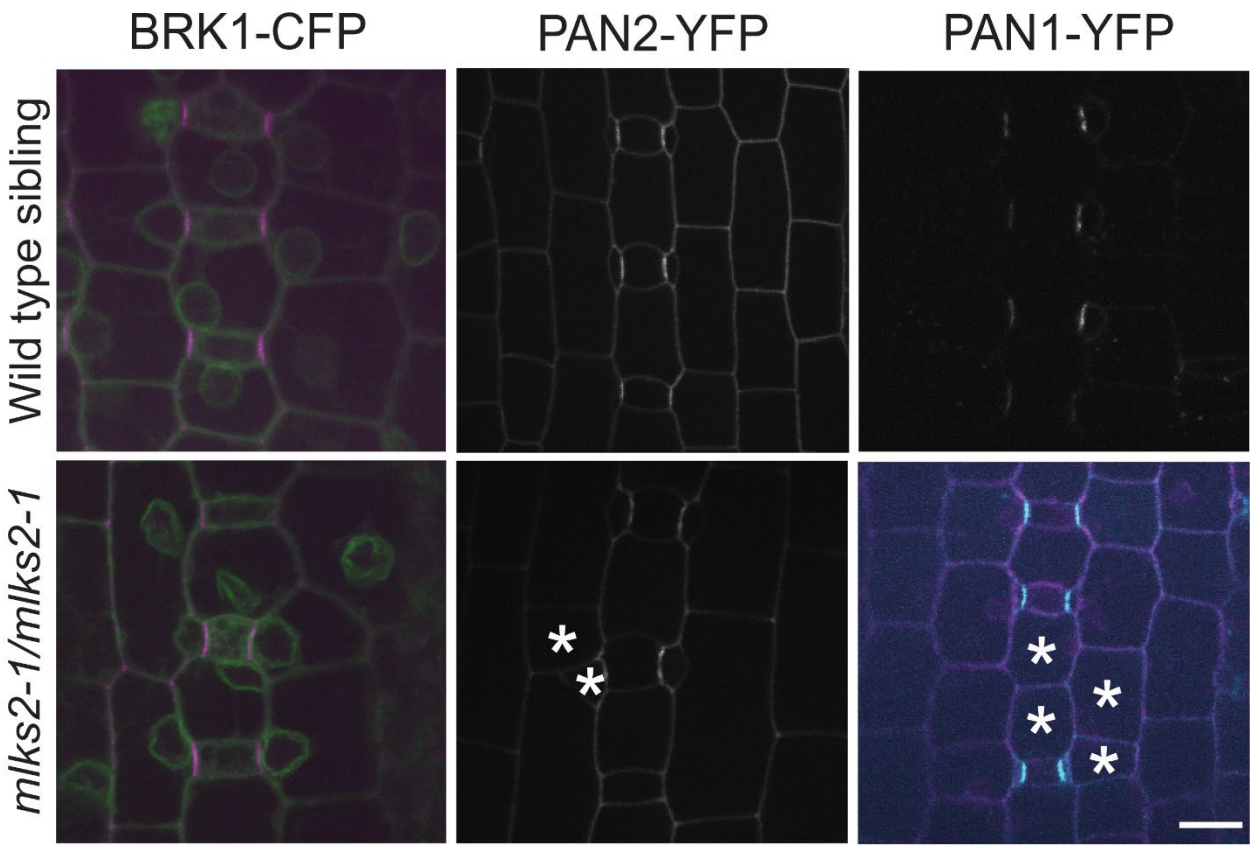

Supplemental Figure S5. Earlier cell polarity markers remain the same in *mlks2-1*. Localization of BRK1-CFP (with RanGAP-YFP), PAN2-YFP, and PAN1-YFP (with CFP-TUB) in wild type (upper panel) and *mlks2-1* (lower panel). Pseudocolor: BRK1-CFP as magenta, RanGAP-YFP as green, PAN1-YFP as cyan, and CFP-TUB as blue. Scale bar = 10 μm.

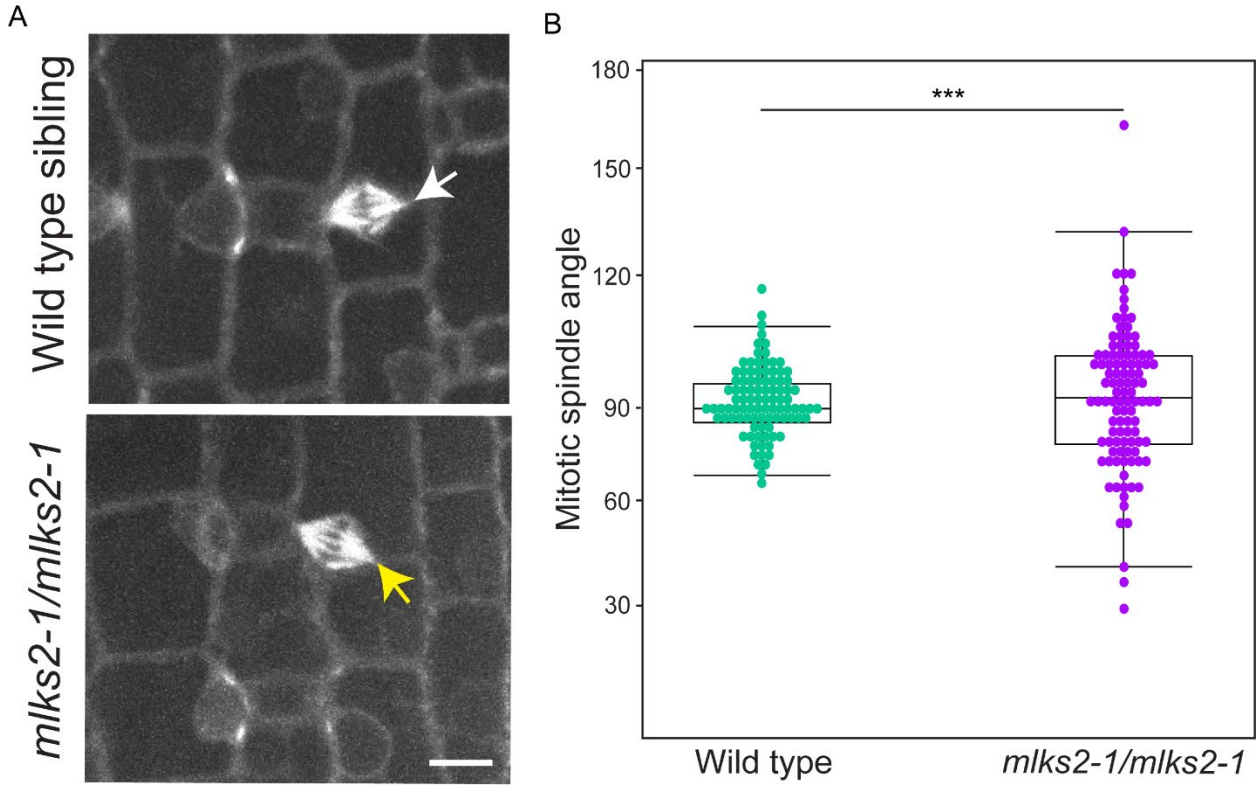

Supplemental Figure S6. Mitotic spindle angle is altered in the *mlks2-1*. A, Mitotic spindle morphology is observed using CFP-TUB for wild type sibling and *mlks2-1*. White arrow indicates the mitotic spindle with an angle close to 90^0. Yellow arrow indicates the mitotic spindle deviated from ideal 90^0. Scale bar = 10 µm. B, Spindle angle was quantified. At least 3 plants from each genotype are used for the experiment. 96 wild type and 104 *mlks2-1* cells were considered for the quantification. The total number of cells judged statistically based on mean (P=0.5169) and variance (P<0.0001) by 2-sided F-test. ***P <0.0001.

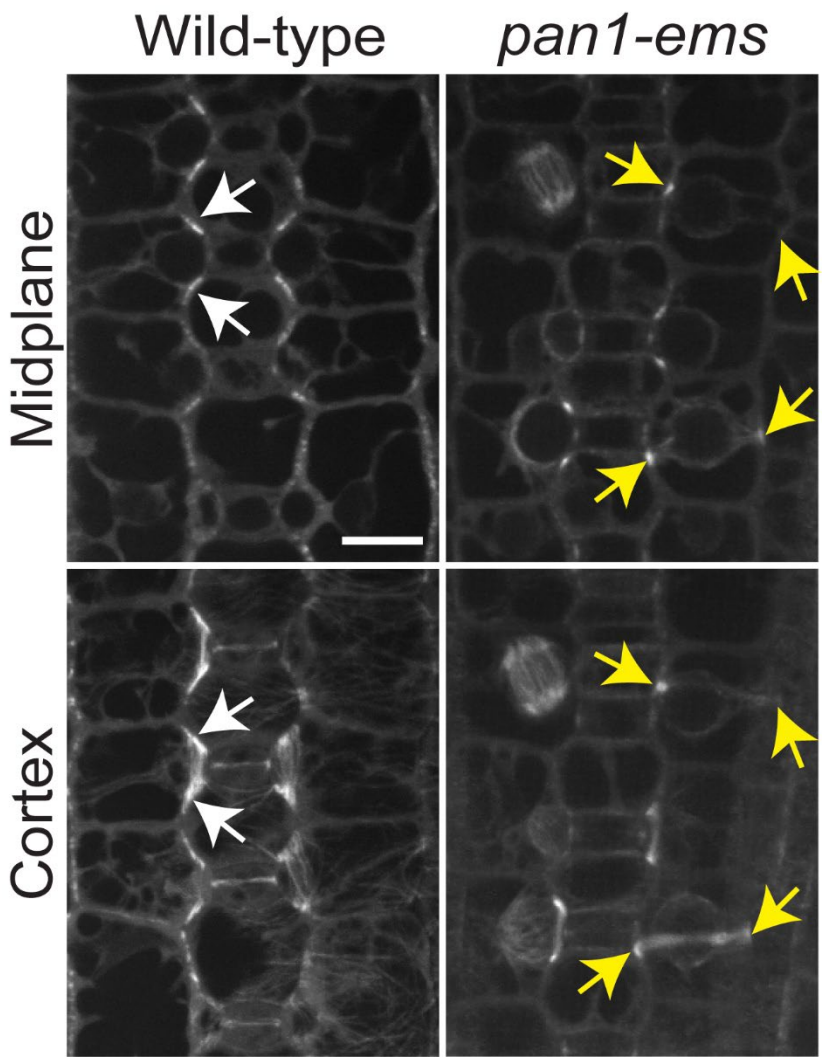

Supplemental Figure S7. Transverse PPB formation in the *pan1-ems*. Observation of PPB using YFP-TUB in wild type and *pan1-ems* from the midplane and cortex. White and yellow arrow indicate perfectly placed and misplaced PPB, respectively. At least 3 plants from each genotype and ~100 cells from each plant were observed. Scale bar = 10 μm.

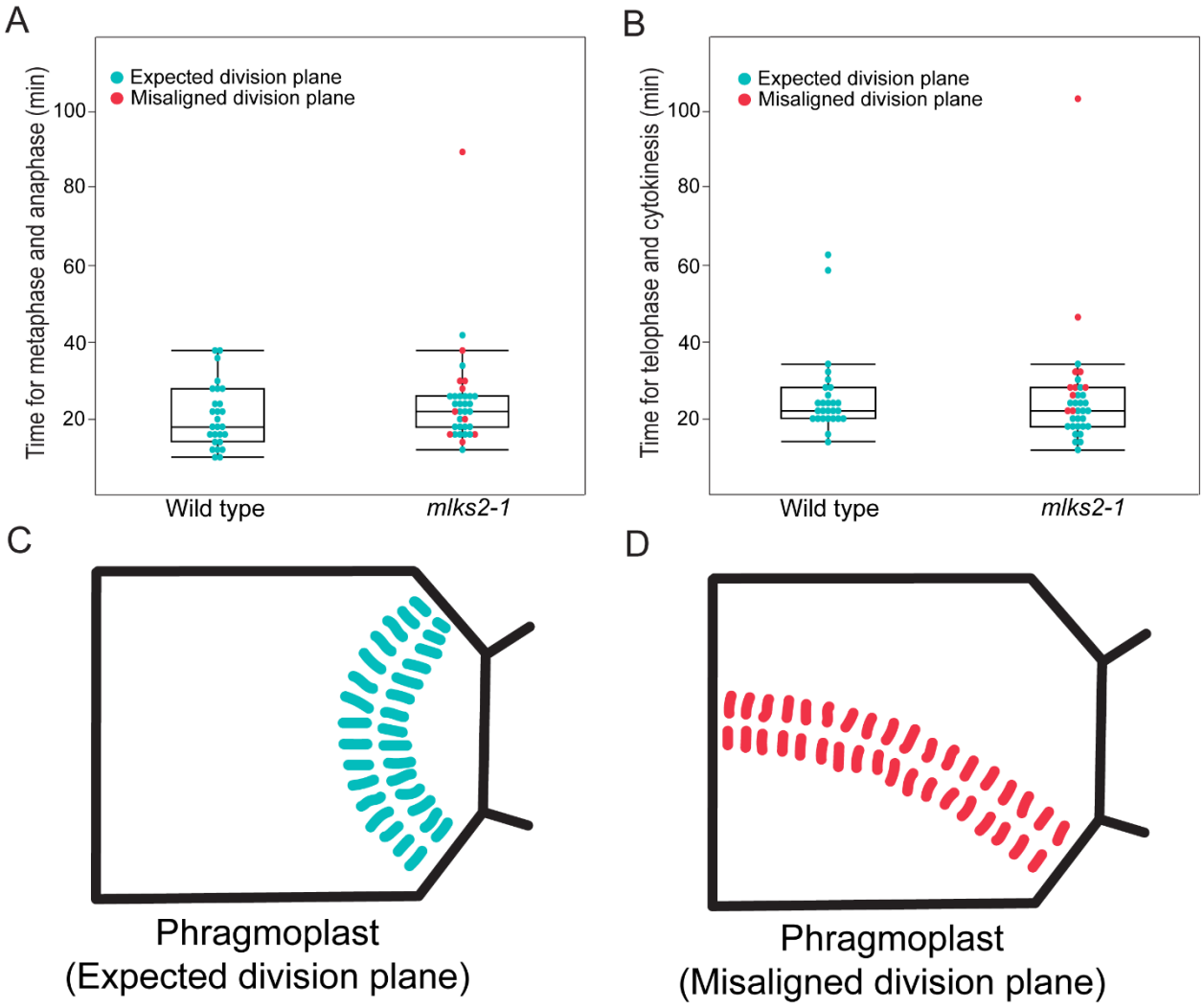

Supplemental Figure S8. Telophase and cytokinesis require longer time in *mlks2-1*. Duration of mitosis is divided into: metaphase + anaphase; telophase + cytokinesis. Duration of metaphase + anaphase (A) and telophase + cytokinesis (B) from the observed time lapse movies, related to Figure 6. Cyan and red dot indicate cells with expected division plane and misaligned division plane, respectively, from both wild type and *mlks2-1*. C, Cartoon shows the shortest path covered by phragmoplast for cells with expected division plane. D, Comparatively longer path is covered by phragmoplast for cells with misaligned division plane.

Supplementary Movie Legends

Supplemental Movie S1. MLKS2 localizes at the nuclear membrane and with phragmoplast and new cell plate. Transient tobacco expression with pCaMV35S::MLKS2-mNG and pCaMV35S::AtCYCD3. Time lapse movie was captured after 48h of the transformation. The images were captured in every 2 min interval.

Supplemental Movie S2. Asymmetric cell division in wild type cell. HIS-YFP (magenta) and CFP-TUB (green) were used for the visualization of nucleus and microtubules, respectively. The images were captured in every 2 min interval.

Supplemental Movie S3. Transverse PPB placement with an offset nucleus leads to aberrant asymmetric cell division in *mlks2-1*. HIS-YFP (magenta) and CFP-TUB (green) were used for the visualization of nucleus and microtubules, respectively. The images were captured in every 2 min interval.

Supplemental Movie S4. Nucleus locks with PPB in the wild type cell. HIS-YFP (magenta) and CFP-TUB (green) were used for the visualization of nucleus and microtubules, respectively. The images were captured in every 2 min interval.

Supplemental Movie S5. Unpolarized nucleus locks with misplaced PPB in *mlks2-1* cell. HIS-YFP (magenta) and CFP-TUB (green) were used for the visualization of nucleus and microtubules, respectively. The images were captured in every 2 min interval.

Supplemental Movie S6. Polarized nucleus with perfectly placed PPB moves away in *mlks2-1* cell. CFP-TUB, as green, marks PPB and nucleus. PAN2-YFP, as magenta, localizes at the GMC-SMC interphase. The images were captured in every 2 min interval.

Supplemental Movie S7. Nuclear movement in wild type cell prior to PPB formation. HIS-YFP (magenta) and CFP-TUB (green) were used for the visualization of nucleus and microtubules, respectively. The images were captured in every 2 min interval.

Supplemental Movie S8. Nuclear movement in *mlks2-1* cell prior to PPB formation. HIS-YFP (magenta) and CFP-TUB (green) were used for the visualization of nucleus and microtubules, respectively. The images were captured in every 2 min interval.

Supplemental Table S1. Primers used in this study for genotyping and cloning.

Primer	Identifier	Sequence
MF03	TIR6	agagaagccaacgccawsgcctcyatttcgtc
MF533	mlks21_gF1	ggaggcgtacgcgaggtcca
MF534	mlks21_gR1	gaggctccggcatgggctct
MF535	mlks22_gF2	attcatccatcatgaacggcagcac
MF536	mlks22_gR2	ctgggactgggagtcttgtcccttg
AA106	MLKS2_fwd_for_mNG	ggctac**cacctgc**agcg***ctgg***GGGGACAAGTTTGTACAAAAAAGC
AA107	MLKS2_rev_for_mNG	ggctac**cacctgc**ttcc***TCCA***GCAGTGGGGACAAG
AA108	mNeonGreen_fwd	ggctac**cacctgc**ttcc***tgga***gctgctgcaGCTGGTGCAATGGTGAGC
AA109	mNeonGreen_rev	ggctac**cacctgc**tgcg***atgc***GGGGACCACTTTGTACAAG
AA98	MLKS2_attB1_F	GGGGACAAGTTTGTACAAAAAAGCAGGCTATGGGCCGGAGCCTGAGCCCGC
AA47	mNG_attB2_R	GGGGACCACTTTGTACAAGAAAGCTGGGTtcaCTTGTACAGCTCGTCCATGCC